

lek. Marta Hałaburda- Rola

Zastosowanie kliniczne tomografii komputerowej wysokiej rozdzielczości (HRCT) w diagnostyce płucnych powikłań infekcyjnych u chorych z chorobami hematologicznymi.

**Rozprawa na stopień doktora nauk medycznych i nauk o zdrowiu
w dyscyplinie nauki medyczne**

Promotor: Dr hab. n. med. Laretta Grabowska- Derlatka

Zakład: II Zakład Radiologii Klinicznej



Obrona rozprawy doktorskiej przed Radą Dyscypliny Nauk Medycznych
Warszawskiego Uniwersytetu Medycznego

Warszawa 2023 r.

Słowa kluczowe w języku polskim:

Tomografia komputerowa

Radiologia

Inwazyjna aspergiloza płucna

COVID-19

Choroby zakaźne

Immunosupresja

Nowotwory hematologiczne

Słowa kluczowe w języku angielskim:

Computed tomography

Radiology

Invasive pulmonary aspergillosis

COVID-19

Infectious diseases

Immunosuppression

Hematological malignancies

Mojemu Tacie.

Wykaz publikacji stanowiących pracę doktorską:

1. **Hałaburda-Rola M**, Dzieciatkowski T, Górka M, Rowiński O, Grabowska-Derlatka L. Clinical utility of the updated European Organization for Research and Treatment of Cancer/Invasive Fungal Infections Cooperative Group and the National Institute of Allergy and the Mycoses Study Group Education and Research Consortium computed tomography criteria of invasive pulmonary aspergillosis in hematological malignancies. *Hematology*. 2021 Dec;26(1):398-407. doi: 10.1080/16078454.2021.1931739. IF: **2,264** MEiN: **40 pkt.**
2. **Hałaburda-Rola M**, Drozd-Sokołowska J, Januszewicz M, Grabowska-Derlatka L. Comparison of Computed Tomography Scoring Systems in Patients with COVID-19 and Hematological Malignancies. *Cancers*. 2023; 15(9):2417. <https://doi.org/10.3390/cancers15092417> IF: **5,2** MEiN: **200 pkt.**

Łączna punktacja IF: **7,464**

Łączna punktacja MEiN: **240 pkt.**

Spis treści:

1. Wykaz stosowanych skrótów.....	6
2. Streszczenie w języku polskim	7
3. Streszczenie w języku angielskim.....	10
4. Wstęp.....	14
5. Założenia i cel pracy.....	18
6. Kopie opublikowanych prac.....	19
7. Wnioski.....	50
8. Opinie Komisji Bioetycznej.....	51
9. Oświadczenia wszystkich współautorów publikacji określające indywidualny wkład każdego z nich w ich powstanie.....	53

1. Wykaz stosowanych skrótów (w kolejności alfabetycznej)

TKWR	Tomografia komputerowa wysokiej rozdzielczości (<i>High resolution computed tomography</i>)
EORTC/MSG	Grupa badawcza Europejskiej Organizacji Badań i Leczenia Grzybic Nowotworowych (<i>European Organisation for Research and Treatment for Cancer Mycoses Study Group</i>)
IPA	Inwazyjna aspergiloza płucna (<i>Invasive pulmonary aspergillosis</i>)
GGO	Zagęszczenia o typie matowej szyby (<i>Ground glass opacities</i>)
COVID-19	Choroba wywołana zakażeniem koronawirusem Sars- Cov-2 (<i>Coronavirus Disease 2019</i>)
BAL	Popłuczyny oskrzelowo- pęcherzykowe (<i>Broncho-alveolar lavage</i>)

2. Streszczenie w języku polskim

Wstęp

Tomografia komputerowa wysokiej rozdzielczości (TKWR) jest powszechnie stosowaną metodą diagnostyki obrazowej umożliwiającą rozpoznawanie powikłań infekcyjnych w płucach. Tomografia komputerowa wysokiej rozdzielczości jest badaniem obiektywnym, powtarzalnym i łatwo dostępnym. Znajomość objawów radiologicznych typowych dla infekcji płucnych w odniesieniu do obowiązujących kryteriów diagnostycznych koreluje z rokowaniem dla pacjenta oraz przekłada się bezpośrednio na postępowanie kliniczne.

Publikacja nr 1 wchodząca w skład cyklu rozprawy doktorskiej

Hałaburda-Rola M, Dzieciatkowski T, Górka M, Rowiński O, Grabowska-Derlatka L. Clinical utility of the updated European Organization for Research and Treatment of Cancer/Invasive Fungal Infections Cooperative Group and the National Institute of Allergy and the Mycoses Study Group Education and Research Consortium computed tomography criteria of invasive pulmonary aspergillosis in hematological malignancies. Hematology. 2021 Dec;26(1):398-407. doi: 10.1080/16078454.2021.1931739.

Niniejszy artykuł stanowi oryginalną pracę badawczą, której celem była analiza klinicznej przydatności zaktualizowanych kryteriów European Organisation for Research and Treatment for Cancer Mycoses Study Group (EORTC/MSG) dotyczących rozpoznawania inwazyjnej aspergilozy płucnej (IPA) na podstawie kryteriów radiologicznych, u pacjentów z chorobami hematologicznymi. W pracy zawarty został przegląd literatury, szeroko omówiono zagadnienie radiologicznych objawów oraz przedstawiono szczegółowo kryteria rozpoznania IPA.

Materiał badawczy stanowiły wyjściowe badania TKWR u pacjentów z chorobami hematologicznymi i z klinicznym podejrzeniem IPA.

Do badania włączono 35 pacjentów, u których wykonano badania TKWR 64-rzędowym tomografem komputerowym, na pełnym wdechu, jednofazowo, bez podania środka kontrastującego. Badania włączone do analizy były w pełni zanonimizowane i oceniane przez dwóch niezależnych badaczy pod kątem jakościowym, lokalizacji oraz wielkości zmian. Przypadki dyskusyjne były konsultowane z trzecim, niezależnym badaczem. Analiza jakościowa zawierała ocenę objawów radiologicznych typowych dla IPA takich jak dobrze

odgraniczone zagęszczenia guzkowe z halo lub bez, objaw „powietrznego rąbka w kształcie półksiężyca”, kawitacje, a także nowego kryterium rozpoznania IPA- skonsolidowanych zagęszczeń mięsaszowych segmentalnych lub subsegmentalnych, klinowatego kształtu. Ponadto, notowane były radiologiczne objawy nietypowe dla IPA, takie jak zagęszczenia o typie matowej szyby (GGO), płyn w jamach opłucnowych, pogrubienie przegród międzyzrazikowych oraz limfadenopatia śródpiersia.

U wszystkich pacjentów w grupie badanej stwierdzono typowe, radiologiczne objawy IPA. Najczęstszymi radiologicznymi objawami były zagęszczenia guzkowe otoczone halo lub bez, które występowały u 88.5% pacjentów. U 60% pacjentów rozpoznano objawy radiologiczne nietypowe dla IPA, takie jak GGO, płyn w jamach opłucnowych, pogrubienie przegród międzyzrazikowych oraz limfadenopatię śródpiersia, występujące odpowiednio u 31.4%, 34.3%, 14.3%, 11.4% populacji. Skonsolidowane zagęszczenia mięsaszowe segmentalne lub subsegmentalne klinowatego kształtu występowały u 48.6% pacjentów, przy czym u 11.4% pacjentów były jedynymi objawami radiologicznymi typowymi dla IPA.

Zaktualizowane kryteria radiologiczne zaproponowane przez EORTC/MSG włączają klinowate segmentalne lub subsegmentalne obszary zagęszczeń mięsaszowych jako jeden z typowych objawów radiologicznych IPA. Na podstawie przedstawionych wyników w naszym badaniu wykazano, że aktualizacja kryteriów radiologicznych umożliwiła postawienie rozpoznania prawdopodobnej aspergilozy płucnej u 11.4% pacjentów więcej w porównaniu z poprzednią klasyfikacją.

Publikacja nr 2 wchodząca w skład cyklu rozprawy doktorskiej

Hałaburda-Rola M, Drozd-Sokołowska J, Januszewicz M, Grabowska-Derlatka L. Comparison of Computed Tomography Scoring Systems in Patients with COVID-19 and Hematological Malignancies. Cancers. 2023; 15(9):2417. <https://doi.org/10.3390/cancers15092417>

Powyższa publikacja stanowi oryginalną, retrospektywną analizę porównawczą skal półilościowych stosowanych w TKWR do oceny rozległości zajęcia mięszu płucnego przez zmiany patologiczne, występujące w przebiegu infekcji COVID-19 u pacjentów z chorobami hematologicznymi. Do analizy włączono 50 pacjentów z nowotworami hematologicznymi oraz z potwierdzonym zakażeniem COVID-19. U wszystkich badanych wykonano TKWR klatki piersiowej, jednofazowo, bez podania środka kontrastującego, na pełnym wdechu. Do analizy

obrazów tomografii komputerowej wykorzystano trzy skale ilościowe tj. CT Severity Score, CT Score i Total Severity Score oraz jedną skalę jakościową- modified Total Severity Score. Badania poddane analizie były w pełni zanonimizowane i interpretowane przez dwóch lekarzy radiologów z wieloletnim doświadczeniem w ocenie obrazów tomografii komputerowej klatki piersiowej u pacjentów hematologicznych. W analizie uwzględniono następujące parametry: czas interpretacji obrazów w danej skali, zgodność pomiędzy obserwatorami w interpretacji obrazów oraz czułość i swoistość wybranych skal w rozpoznawaniu COVID-19 o przebiegu ciężkim i lekkim. Na podstawie interpretacji badań, uzyskano następujące wyniki: CT Score i Chest CT Severity Score cechują się bardzo wysoką czułością i swoistością pod względem dokładności diagnostycznej. Ponadto, biorąc pod uwagę najkrótszą medianę czasu analizy w skali CT Severity Score można wnioskować, że metoda ta jest preferowana w ocenie TKWR klatki piersiowej u pacjentów hematologicznych z COVID-19.

Podsumowanie

Przedstawione wyniki prac stanowiących cykl publikacji tworzących rozprawę doktorską dowodzą, że TKWR jest cenną metodą obrazową w rozpoznawaniu powikłań infekcyjnych u pacjentów hematologicznych. Umiejętność interpretacji obrazów TKWR klatki piersiowej w oparciu o najnowsze kryteria diagnostyczne rozpoznawania IPA, pozwala na postawienie diagnozy u większego odsetka pacjentów, co przekłada się bezpośrednio na postępowanie kliniczne. W przypadku pacjentów z chorobami hematologicznymi i z infekcją COVID-19, obiektywna, ilościowa wystandaryzowana ocena stopnia zajęcia mięszu płucnego koreluje ze stanem klinicznym pacjenta i wpływa się na postępowanie terapeutyczne.

3. Streszczenie w języku angielskim

Introduction:

High-resolution computed tomography (HRCT) is a widely used diagnostic imaging method for diagnosing infectious complications in the lungs. HRCT is an objective, reproducible and broadly available method. Knowledge of the radiological signs typical of pulmonary infections in relation to the current diagnostic criteria correlates with the prognosis for the patient and correlates directly with clinical management.

Manuscript #1 in the dissertation series

Hałaburda-Rola M, Dzieciatkowski T, Górka M, Rowiński O, Grabowska-Derlatka L. Clinical utility of the updated European Organization for Research and Treatment of Cancer/Invasive Fungal Infections Cooperative Group and the National Institute of Allergy and the Mycoses Study Group Education and Research Consortium computed tomography criteria of invasive pulmonary aspergillosis in hematological malignancies. Hematology. 2021 Dec;26(1):398-407. doi: 10.1080/16078454.2021.1931739.

This article is an original research paper that aimed to analyze the clinical usefulness of the updated EORTC/MSG criteria for the diagnosis of IPA based on radiological criteria, in patients with hematological diseases. The paper included a literature review, extensively discussed the issue of radiological manifestations and detailed the criteria for the diagnosis of IPA.

The study material consisted of baseline HRCT of patients with hematological diseases, neutropenia and clinically suspected IPA.

All HRCT were performed on a 64-row CT scanner, on full inspiration, single-phase, without contrast agent administration. Studies included in the analysis were fully anonymized and evaluated by two independent radiologists for quality, location and size of lesions. The differences in interpretation were resolved by third, independent radiologist. Qualitative analysis included evaluation of radiological signs typical of IPA such as well-defined nodules with or without halo, the air crescent sign and cavitations, as well as the new criterion for the diagnosis of IPA- wedge-shaped segmental or subsegmental consolidations. In addition, radiologic signs atypical of IPA such as ground glass opacities (GGO), pleural fluid, thickening of interlobular septa and mediastinal lymphadenopathy were noted. All patients in the study group had typical radiological signs of IPA and met the criteria of probable IPA. The most

common radiological signs were nodules with halo, which were present in 88.5% of patients. Radiological signs atypical of IPA, such as GGO, pleural fluid, thickening of interlobular septa, mediastinal lymphadenopathy, were diagnosed in 60% of patients, occurring in 31.4%, 34.3%, 14.3%, 11.4% of the population, respectively. Segmental or subsegmental wedge-shaped consolidations were present in 48.6% of patients, with 11.4% constituting the only radiological signs of IPA. Based on the results, it can be concluded, the updated radiological criteria allowed the diagnosis of probable IPA in 11.4% more patients in comparison to the previous classification.

Manuscript #2 in the dissertation series

Hałaburda-Rola M, Drozd-Sokołowska J, Januszewicz M, Grabowska-Derlatka L. Comparison of Computed Tomography Scoring Systems in Patients with COVID-19 and Hematological Malignancies. Cancers. 2023; 15(9):2417. <https://doi.org/10.3390/cancers15092417>

The publication is an original, retrospective comparative analysis of semiquantitative scales used in HRCT to assess the extent of pulmonary parenchymal involvement by lesions occurring in the course of COVID-19 infection in patients with hematological diseases. Fifty patients with hematologic malignancies and confirmed COVID-19 infection were included in the analysis, and all patients underwent chest HRCT without contrast agent administration, on full inspiration. Three semi-quantitative scales, i.e., CT Severity Score, CT Score and Total Severity Score, and one qualitative scale, the modified Total Severity Score, were used to analyze HRCT images. The studies analyzed were fully anonymized and interpreted by two radiologists with the experience in interpreting chest CT images in hematology patients. The time of analysis, interobserver concordance and the sensitivity and specificity of the selected scales in diagnosing COVID-19 with severe and mild disease were analyzed. Based on the interpretation of the studies, the following results were obtained: Chest CT score and Chest CT Severity Score have very high sensitivity and specificity in terms of diagnostic accuracy. Additionally, considering the shortest median of the interpretation time in the chest CT Severity Score, the method can be proposed as dedicated for semi-quantitative assessment of chest CT in hematological patients with COVID-19.

Conclusions

The presented results of the work constituting the series of publications forming the dissertation prove that HRCT is an indispensable imaging method in the diagnosis of infectious complications in hematological patients. The ability to interpret HRCT images of the chest based on the latest diagnostic criteria for the diagnosis of probable IPA, allows the diagnosis to be made in a higher percentage of patients, which translates directly into clinical management. For patients with hematologic diseases and COVID-19 infection, an objective, semi-quantitative standardized assessment of the degree of pulmonary parenchymal involvement correlates with the patient's clinical status and translates into therapeutic management of the patient.

Rozprawa doktorska- cykl publikacji

Zastosowanie kliniczne tomografii komputerowej wysokiej rozdzielczości w diagnostyce płucnych powikłań infekcyjnych u chorych z chorobami hematologicznymi.

4. Wstęp

Pacjenci z nowotworami hematologicznymi są w grupie ryzyka rozwoju powikłań infekcyjnych zarówno bakteryjnych, wirusowych jak i grzybiczych, ze względu na zaburzenia odporności występujące w przebiegu choroby podstawowej bądź jako powikłanie leczenia. Jedną z częstszych infekcji u chorych hematologicznych jest inwazyjna aspergiloza płucna (IPA), wywołana przez grzyb z rodzaju kropidlakowców *Aspergillus spp.* Choroba wywołana jest naciekiem ściany oskrzela oraz towarzyszących naczyń tętniczych przez strzępki grzyba. Do czynników predysponujących do rozwoju IPA należą choroby hematologiczne, w szczególności ostra i przewlekła białaczka szpikowa, chemioterapia, sterydoterapia, leczenie immunosupresyjne oraz przeszczepienie szpiku kostnego. Szczególnie narażeni są pacjenci z poziomem neutrofilii we krwi obwodowej $<500/uL$.

Wzrost częstości stosowania chemioterapii oraz leczenia immunosupresyjnego na przestrzeni ostatnich 30 lat spowodował wzrost zachorowań na inwazyjną grzybicę płucną z 0.4% na 3.1% w populacji ogólnej oraz podwyższenie odsetka pacjentów z rozpoznaniem IPA z 18% do 65% wśród wszystkich inwazyjnych grzybic płucnych. Ze względu na wysoką śmiertelność, przekraczającą 50% u pacjentów nieleczonych, konieczna jest szybka i miarodajna diagnostyka w celu wdrożenia odpowiedniego leczenia.

Na podstawie najnowszych kryteriów European Organisation for Research and Treatment for Cancer Mycoses Study Group criteria (EORTC/MSG criteria), rozpoznanie IPA kategoryzuje się jako możliwe, prawdopodobne bądź pewne, w zależności od czynników ryzyka, objawów klinicznych, radiologicznych i mikrobiologicznych. U pacjentów, u których pobrano biopsję zmian podejrzanych i w badaniu histopatologicznym uwidoczniono strzępki grzybni rozpoznanie można postawić w stopniu pewnym. Rozpoznanie w stopniu prawdopodobnym możliwe jest w przypadku obecnych czynników ryzyka IPA, obecności strzępków grzybi w badaniu mikroskopowym pobranym z popłuczyn oskrzelowo-pęcherzykowych (BAL), biopsji szczoteczkowej oskrzeli bądź płwociny lub stwierdzenia obecności dodatnich antygenów grzybiczych we krwi obwodowej i BAL. Rozpoznanie w stopniu możliwym można postawić u pacjentów z immunosupresją, z dodatnimi objawami klinicznymi, przy braku dodatnich objawów mikrobiologicznych. Dobrze poznane i opisane w literaturze radiologiczne objawy IPA w TKWR to: dobrze odgraniczone zagęszczenia guzkowe otoczone halo lub bez, objaw „powietrznego rąbka w kształcie półksiężyca” oraz kawitacje.

Zaktualizowana wersja kryteriów EORTC/MSG z 2020 roku, oprócz powyżej opisywanych objawów radiologicznych IPA, włącza obszary klinowych, segmentalnych bądź płatowych zagęszczeń miąższowych jako nowe, możliwe radiologiczne objawy IPA. W naszej pracy skupiliśmy się na nowym i dotychczas nieopisanym zagadnieniu jakim jest zastosowanie kliniczne zaktualizowanych kryteriów EORTC/MSG. Pierwsza praca prezentowanego cyklu (*Hałaburda-Rola M, Dzieciatkowski T, Górka M, Rowiński O, Grabowska-Derlatka L. Clinical utility of the updated European Organization for Research and Treatment of Cancer/Invasive Fungal Infections Cooperative Group and the National Institute of Allergy and the Mycoses Study Group Education and Research Consortium computed tomography criteria of invasive pulmonary aspergillosis in hematological malignancies. Hematology. 2021 Dec;26(1):398-407. doi: 10.1080/16078454.2021.1931739.*) jest pracą oryginalną i stanowi retrospektywną analizę TKWR u pacjentów z nowotworami hematologicznym i neutropenią. W pracy opisano objawy kliniczne oraz omówiono czynniki ryzyka rozwoju IPA. Ponadto szczegółowo zostały przedstawione najnowsze radiologiczne kryteria diagnostyczne oraz szeroko zostały opisane zmiany radiologiczne występujące w przebiegu IPA. Podkreślono istotność nowego objawu radiologicznego jakim są zagęszczenia miąższowe klinowatego kształtu. W naszym materiale objaw ten notowano u 48.6% pacjentów, przy czym u 11.4% był to jedyny objaw radiologiczny IPA. Zwrócono uwagę na trudności diagnostyczne w interpretacji obrazów TKWR. Objawy radiologiczne opisane w kryteriach EORTC/MSG mogą współwystępować wraz z objawami nietypowymi dla IPA. Zagęszczenia miąższowe klinowatego kształtu mogą występować również w przebiegu zakażeń bakteryjnych, zatorów septycznych bądź krwawienia do miąższu płucnego.

Guzkowe zagęszczenia z halo lub bez, opisywane w TKWR u pacjentów z zaburzeniami odporności i z czynnikami ryzyka rozwoju IPA mają wysoką wartość predykcyjną dla rozpoznania choroby. W populacji ogólnej zmiany te często występują w innych sytuacjach klinicznych m.in. w przebiegu infekcji o innej etiologii, w tym wirusowej. Nowy wirus Sars-Cov-2, opisany w 2019 roku, który spowodował pandemię COVID-19, ogłoszoną w marcu 2020, stanowi wyzwanie diagnostyczne i terapeutyczne. Z dotychczasowych doniesień wynika, że infekcje COVID-19 u pacjentów hematologicznych mogą mieć nietypowy, przewlekły przebieg, a także cechują się wysoką śmiertelnością, sięgającą 50%. Radiologiczne objawy infekcji COVID-19 są podobne do objawów innych infekcji wirusowych i zmieniają się wraz z czasem trwania infekcji. Początkowo występują zagęszczenia o typie „matowej szyby”, najczęściej zlokalizowane obwodowo, symetrycznie w płatach dolnych oraz zmiany o typie kostki brukowej z pogrubieniem przegród śródzrazikowych. W okresie od około 7 do 14 dni

od początku wystąpienia infekcji pojawiają się zmiany o typie zagęszczeń miąższowych, natomiast objawami późnymi są zmiany włókniste i rozstrzenia oskrzeli. Zwłóknienia zazwyczaj ustępują powoli i obserwowane są w odległych badaniach kontrolnych.

Objawy radiologiczne choroby COVID-19 są nieswoiste. Zgodnie z zaleceniami Fleischner Society, TKWR nie jest metodą diagnostyczną zalecaną do rozpoznania choroby, natomiast jest wskazana u pacjentów z potwierdzoną infekcją COVID-19 u których doszło do pogorszenia wydolności oddechowej, a także u osób z łagodnymi objawami klinicznymi, u których istnieje duże ryzyko progresji choroby, między innymi u pacjentów z immunosupresją. U osób zakażonych COVID-19, ze wskazaniem do wykonania diagnostyki obrazowej, badaniem zalecanym jest tomografia komputerowa wysokiej rozdzielczości TKWR klatki piersiowej bez podania środka kontrastującego, natomiast w uzasadnionych przypadkach, szczególnie u pacjentów z podejrzeniem powikłań, takich jak zatorowość płucna, badanie można dodatkowo wykonać ze środkiem kontrastującym. TKWR umożliwia ocenę stopnia zajęcia miąższu płucnego, rozpoznania ewentualnych powikłań bądź współistniejących infekcji. Druga praca prezentowanego cyklu (*Hałaburda-Rola M, Drozd-Sokołowska J, Januszewicz M, Grabowska-Derlatka L. Comparison of Computed Tomography Scoring Systems in Patients with COVID-19 and Hematological Malignancies. Cancers. 2023; 15(9):2417. <https://doi.org/10.3390/cancers15092417>*) stanowi pierwszą opublikowaną analizę porównawczą skal stosowanych do oceny rozległości zmian w miąższu płucnym w przebiegu COVID-19 u pacjentów z nowotworami hematologicznymi. W pracy omówiono wskazania do wykonania diagnostyki obrazowej u pacjentów z COVID-19, przedstawiono objawy radiologiczne COVID-19, diagnostykę różnicową oraz opisano szczegółowo trzy skale półilościowe oraz jedną skalę jakościową wykorzystane w analizie.

Ocena TKWR klatki piersiowej pacjentów z nowotworami hematologicznymi jest trudna, wymaga znajomości objawów radiologicznych występujących w chorobach hematologicznych i niejednokrotnie wiedzy klinicznej dotyczącej podstawowej jednostki chorobowej, czynników ryzyka rozwoju powikłań infekcyjnych i stosowanego leczenia. Przedstawione publikacje potwierdzają zasadność stosowania najnowszych kryteriów rozpoznawania inwazyjnej aspergilozy płucnej u chorych hematologicznych oraz sugerują zastosowanie skal oceniających zmiany w miąższu płucnym w przebiegu COVID-19 celem bardziej obiektywnej korelacji objawów radiologicznych ze stanem klinicznym pacjentów z chorobami hematologicznymi.

Przedstawiony cykl prac, stanowiący moją rozprawę doktorską, przyczynia się do poszerzenia wiedzy dotyczącej obrazowania w tomografii komputerowej wysokiej rozdzielczości powikłań infekcyjnych u pacjentów hematologicznych.

5. Założenia i cel pracy

1. Celem pracy była ocena przydatności klinicznej tomografii komputerowej wysokiej rozdzielczości u pacjentów z nowotworami hematologicznymi w rozpoznawaniu prawdopodobnej inwazyjnej aspergilozy płucnej według zaktualizowanych kryteriów EORTC/MSG.

2. Analiza porównawcza i wybór najbardziej przydatnej skali służącej ocenie ilościowej zmian w mięszu płucnym u pacjentów hematologicznych z COVID-19.

Clinical utility of the updated European Organization for Research and Treatment of Cancer/Invasive Fungal Infections Cooperative Group and the National Institute of Allergy and the Mycoses Study Group Education and Research Consortium computed tomography criteria of invasive pulmonary aspergillosis in hematological malignancies

Marta Hałaburda-Rola ^a, Tomasz Dzieciatkowski ^{b,c}, Michał Górka^d, Olgierd Rowiński ^a and Lareta Grabowska-Derlatka ^a

^a2nd Department of Radiology, Medical University of Warsaw, Warsaw, Poland; ^bChair and Department of Medical Microbiology, Medical University of Warsaw, Warsaw, Poland; ^cDepartment of Microbiology, Central Clinical Hospital in Warsaw, Warsaw, Poland; ^dDepartment of Hematology, Oncology and Internal Diseases, Medical University of Warsaw, Warsaw, Poland

ABSTRACT

Introduction: Invasive pulmonary aspergillosis is a life-threatening complication in the cases of patients with hematologic malignancies. In December 2019, the European Organization for Research and Treatment of Cancer/Invasive Fungal Infections Cooperative Group and the National Institute of Allergy and the Mycoses Study Group Education and Research Consortium published a revision and an update of the consensus definitions of invasive fungal disease. The aim of this study was to evaluate the signs and radiologic patterns of early-stage invasive pulmonary aspergillosis in computed tomography in patients with hematologic entities according to the latest criteria.

Material and methods: This retrospective analysis of a baseline high-resolution computed tomography included neutropenic patients with hematological malignancies and probable invasive pulmonary aspergillosis. The data were collected between the years 2017 and 2019. Computed tomography was performed within 72 h from the beginning of clinical symptoms: fever, dyspnea or nonproductive cough. CT scans were analyzed by two independent radiologists according to the standardized protocol based on predefined criteria.

Results: All 35 evaluated patients had typical lesions for early-stage invasive aspergillosis. Wedge-shaped infiltrates were noted in 48.6% of patients. In this group, 40% of patients had coexisting atypical radiological findings. In 11.4% of patients, wedge-shape consolidations were noted as the only type of lesions.

Conclusions: Employment of the latest EORTC/MSG criteria increased diagnostic value of the baseline high resolution computed tomography in our study group by 11.4%.

KEYWORDS

Hematology; invasive pulmonary aspergillosis; computed tomography; radiology

Introduction

Invasive pulmonary aspergillosis (IPA) is the most prevalent mold infection. The frequency of IPA is significantly increasing in hematology patients. It is caused by excessive antibiotic therapy, employment of more intensive and immunosuppressive chemotherapy regimens and longer patient survival [1]. IPA is a life-threatening and lethal condition unless promptly diagnosed and treated. One out of the two for early IPA diagnosis is computed tomography.

The incidence of invasive pulmonary aspergillosis is 8% in acute myelocytic leukemia (AML), 6.3% in acute lymphocytic leukemia (ALL), 12.8% in the cases of the patients following allogeneic hematopoietic stem-cell transplantation and 1.1% following autologous hematopoietic stem-cell transplantation [2]. The major risk factors for developing IPA include

neutropenia, prolonged therapy with high-dose corticosteroids, age over 65 and type of hematologic malignancy [3]. In stem cell transplant recipients, other factors such as graft-versus-host disease play a role in the development of IPA [4,5]. Clinical symptoms of IPA are non-specific. Patients usually present with fever, dyspnea, cough and deterioration of clinical condition. Patients may also present with pleuritic chest pain and hemoptysis [6]. Despite the use of mold-active prophylaxis since 1990s, invasive fungal infections remain a leading cause of morbidity in patients with hematological malignancies [7]. The criteria of the European Organization for Research and Treatment of Cancer/Invasive Fungal Infections Cooperative Group and the National Institute of Allergy and the Mycoses Study Group Education and Research Consortium (EORTC/MSG) for diagnosing

CONTACT Marta Hałaburda-Rola  martahalaburdarola@gmail.com

© 2021 The Author(s). Published by Informa UK Limited, trading as Taylor & Francis Group
This is an Open Access article distributed under the terms of the Creative Commons Attribution License (<http://creativecommons.org/licenses/by/4.0/>), which permits unrestricted use, distribution, and reproduction in any medium, provided the original work is properly cited.

IPA are based on clinical features, host factors and microbiological evidence. Depending on which criteria are fulfilled, the diagnosis of an IPA is graded into possible, probable or proven categories. Proven IPA is when histopathologic, cytopathologic or direct microscopic examinations of specimens are positive and clinical, host criteria are met. Probable IPA is when clinical and host criteria are met and galactomannan antigen is detected in serum, plasma, bronchoalveolar lavage (BAL) or cerebrospinal fluid (CSF). Cases that meet the criteria for a host factor and a clinical criteria but mycological criteria are absent are considered possible [8].

The clinical criteria include high-resolution computed tomography (HRCT) evaluation. In IPA, findings such as dense, well-circumscribed lesions with or without a halo sign, air crescent sign, cavity and wedge-shape, segmental or lobar consolidations may occur in HRCT (Figure 1). Consolidations have been included to the criteria lately in the latest revision and an update of the EORTC/MSG criteria (Figure 2) [8].

Early diagnosis and treatment are essential for improving patients' outcome. Proven or probable IPA is associated with a low survival rate of 14% compared to 32% for patients without IPA [9]. The diagnosis of early-stage IPA may be challenging. High resolution computed tomography (HRCT) is a rapid and useful tool for diagnosing IPA. In contrast to bronchoscopy or lung biopsy it is not invasive and easy to perform in patients with

respiratory failure and comorbidities, such as severe thrombocytopenia or hypoxemia [10,11]. Accurate radiological evaluation is essential for the diagnosis of IPA and initiation of anti-fungal treatment.

The aim of this study was to evaluate if the application of updated radiological EORTC/MSG criteria increases the diagnostic value of HRCT.

Materials and methods

Study design and patient population

The data were collected retrospectively from January 2017 to January 2019. The period was chosen due to the availability of updated clinical and microbiological database system. To perform the study we used the following inclusion criteria: hematology patients presenting with clinical symptoms such as fever and lower respiratory tract infection, without any improvement after broad-spectrum antibacterial treatment. In all cases, a HRCT was performed within 72 h from the beginning of the symptoms. None of the patients had a previous history of an invasive mold disease. According to the revised EORTC/MSG criteria, all patients were diagnosed with probable invasive fungal disease, and were started on anti-mold treatment after the baseline HRCT. A follow-up HRCT was performed in all cases within 14 days from the diagnosis. None of the patients had positive bacterial

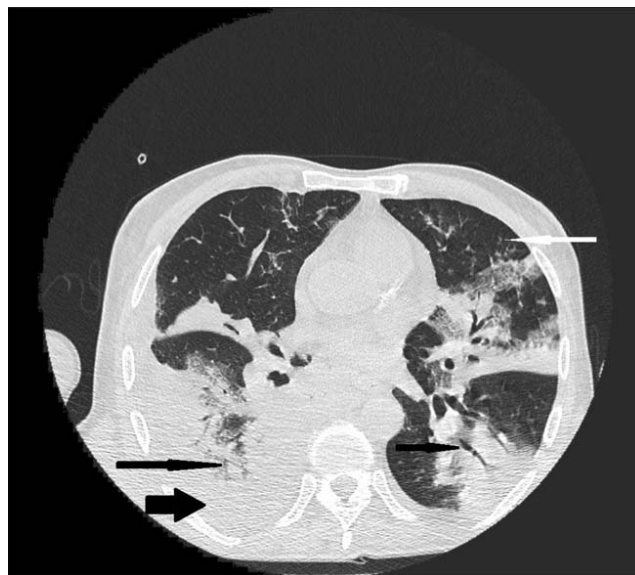


Figure 1. 66-year-old male with chronic lymphocytic leukemia, presenting with crepitations over the lung, cough and fever. High resolution CT scan obtained at level of pulmonary veins shows massive segmental consolidations with air bronchogram located in both lungs (black narrow arrows), nodules with halo sign (white narrow arrow) in lingular segment in left lung and free fluid in right pleural cavity (black wide arrow).

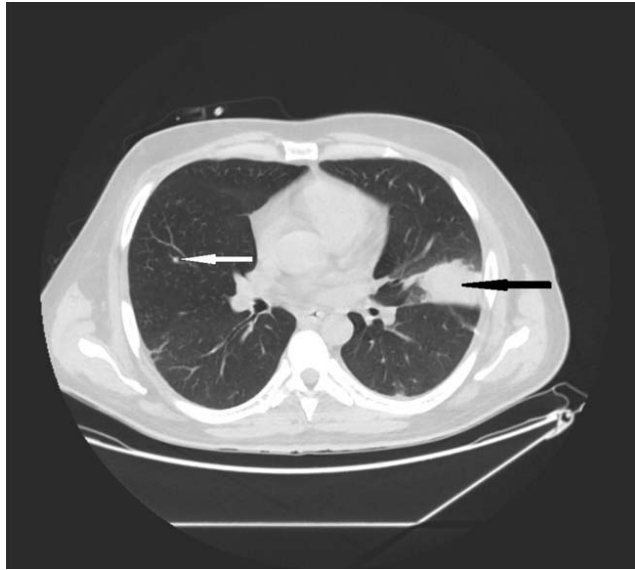


Figure 2. 35-year-old male with acute myeloid leukemia presenting with dry cough. High resolution CT obtained at level of pulmonary veins shows wedge-shape consolidations located in lingular segment in left lung (black narrow arrow). Nodule in the middle lobe of the right lung (white narrow arrow).

blood or sputum cultures nor PCR tests for 15 respiratory viruses (including Influenza, Respiratory Syncytial Virus, Parainfluenza, Metapneumovirus and others) or *Pneumocystis jiroveci* in bronchoalveolar lavage (BAL). Patients with negative galactomannan antigens from serum blood tests or BAL and with mixed etiology of pulmonary infection were excluded from the study. The study was performed according to the seventh revision of Declaration of Helsinki. The Institutional Review Board approved the study. Informed consent was not required due to the retrospective nature of the study.

HRCT scan evaluation

The HRCT scans were acquired using the GE 64-row scanner. The HRCT scans were obtained on supine position at the end-inspiratory effort. The thoracic scanning parameters were 120 kV, 240–460 mA, 1.25 mm collimation and a pitch of 0.984:1 (Table 1). From this dataset axial slices of 1 mm were obtained. The coronal and sagittal slices were as high resolution multiplanar reformation (MPR) images. All HRCT exams were obtained without intravenous contrast administration. Images were analyzed at picture archiving and communications systems (PACS).

The HRCT were reviewed twice and evaluation was made by two independent radiologists (one board specialist with more than 15-year experience in oncologic imaging and one senior resident) according to

standardized protocol based on predefined criteria. The differences in interpretation were resolved by discussion or by the third board certified radiologist. All the clinical data required were accessible to radiologists.

For the study purposes, all pulmonary lesions were analyzed and grouped according to its morphology, size and location (Table 2). The lesions were divided into typical and atypical for IPA in line with the latest criteria. The criteria included typical lesions, such as nodules, nodules with halo, consolidations, air crescent signs and cavities (Figure 3). The atypical findings were as follows: ground glass opacities (GGO), septal thickening, pleural effusions, enlarged lymph nodes.

A standard glossary of terms for computed tomography was applied to describe the lesions [12]:

- nodule was defined as a well marginated round or ovoid shape soft tissue lesion, with the diameter up to 50 mm. Nodules smaller than 10 mm were considered to be micronodules and greater than 50 mm were considered as a consolidation (Figure 4).

Table 1. HRCT acquisition parameters.

HRCT parameters	Value
FOV	Large
Detector coverage (mm)	40.0
Helical thickness (mm)	1.25
Pitch	0.984:1
Rotation time (s)	0.7
Tube voltage (kV)	120
Tube current (mA)	240–460

Table 2. Characteristics of pulmonary findings.

Type of pulmonary findings	Typical for IPA	Atypical for IPA
	Nodule Nodule with halo sign Air crescent sign Cavity Consolidation	Ground glass opacity Septal thickening Pleural effusion Enlarged lymph nodes
Number of lesions		<10
Size of lesions (mm)	Micronodule Nodule Consolidation	≥10 <10 10–50 >50
Location		Central Peripheral

- GGO was defined as hazy increased attenuation of lung with preserved bronchial and vascular margins.
- nodule with halo sign was described as a nodule surrounded by a peripheral rim of GGO (Figures 5 and 6).
- consolidation was considered to be an increase in pulmonary parenchymal attenuation that obscures the airways and vessels.
- wedge- shape consolidations- were considered to be well, sharply marginated, with triangle shape in axial planes (Figures 7 and 8).
- air crescent sign – was the crescentic collection of air surrounding the consolidation or nodule.
- cavity- was a well-defined air space.
- pleural effusion was described as a free fluid in the pleural cavity.

- Other, non-infectious findings such as bronchial wall thickening, bronchiectasis and bullae, were also noted.

The distribution of lesions was considered to be central when located near the central, lobar or segmental bronchi or peripheral when surrounding the subsegmental bronchi (Figure 9).

The radiologists described the number and location of the lesions.

Microbiological analysis

Galactomannan is a highly immunogenic antigen therefore it has been recognized as a good marker of invasive aspergillosis. In soluble form, galactomannan antigen can circulate in body fluids at concentrations of 1–500 ng/ml.

In accordance with the guidelines of EORTC/MSG from 2002 to 2008, serological detection was performed once or twice weekly. *Aspergillus spp.* galactomannan antigen detection was performed using a sandwich immunocapture ELISA (Platelia- *Aspergillus*, Bio- Rad), according to the manufacturer's recommendations in sera samples and/or bronchoalveolar lavage fluid (BALF) specimens. Results were expressed as an index of positivity. They were considered positive when ≥ 0.5 either in sera samples or BALF.

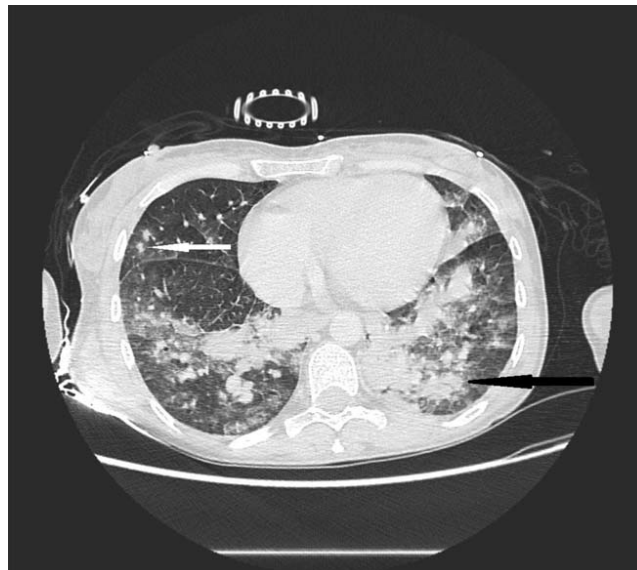


Figure 3. 40-year-old female with cutaneous T-cell lymphoma presenting with fever and dyspnea. High resolution CT scans obtained at level of lower lobes shows consolidations (black narrow arrow) and multiple nodules with halo sign located in both lungs (white narrow arrow).

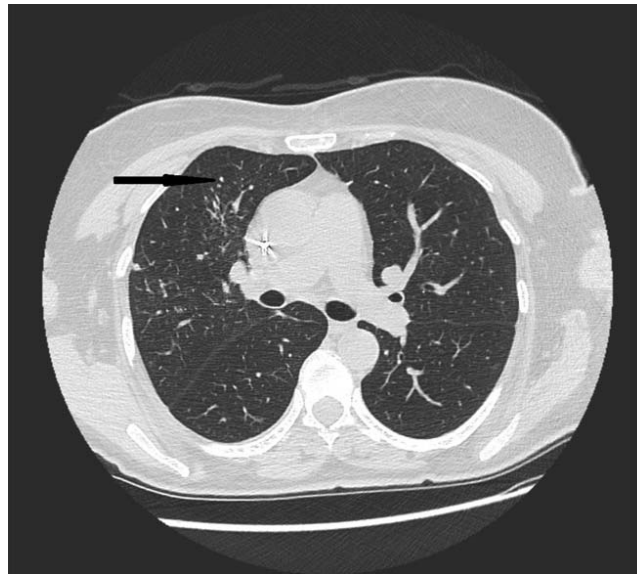


Figure 4. 72-year-old woman with acute myeloid leukemia presenting with fever. High- resolution CT scan obtained at level of main bronchi shows micronodules and nodules located peripherally in middle right lobe (black narrow arrow).

Statistical analysis

The comparative data were analyzed by χ^2 or Fisher's exact test for categorical variables. For the location

and size of lesions a chi-square was applied. A two-sided *p*-value of less than 0.05 was considered statistically significant. All statistical analyses were done with Statistica 13.3 package.



Figure 5. 62-year-old female with acute myeloid leukemia presenting with cough and fever. High resolution CT scan obtained at level of lower lobes shows nodules with halo sign located peripherally in right lower lobe (black narrow arrow).

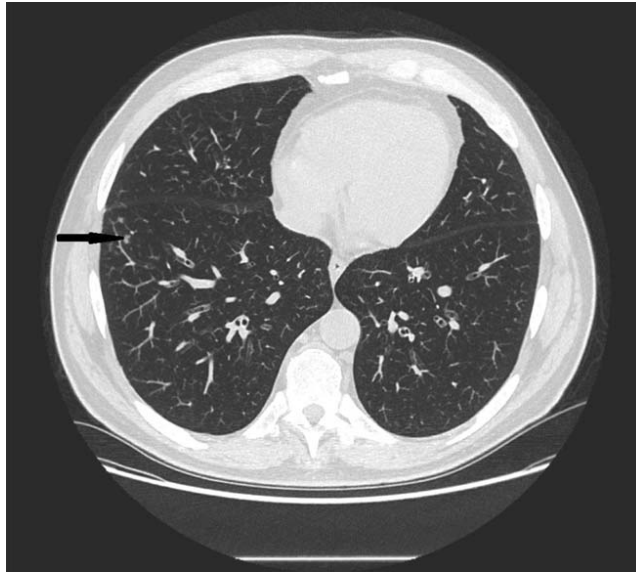


Figure 6. 56-year-old male with primary myeloid fibrosis 30 days after bone marrow transplantation presenting with fever. High resolution CT scan obtained at level of lower lobes shows peripherally located nodules with halo sign in right lower lobe (black narrow arrow).

Results

The study included 35 patients, with a median of 65 (range 22–84), with hematological malignancies and

neutropenia, hospitalized in the Hematology Department of the Medical University of Warsaw between January 2017 and January 2019.



Figure 7. 28-year-old female with congenital neutropenia presenting with productive cough and fever. High resolution CT scans obtained at level of lower lobes shows massive consolidations with air- bronchogram located in basal segments of left lower lobe (black narrow arrow).



Figure 8. 35-year-old male with acute myeloid leukemia presenting with dry cough. High resolution CT in coronal plane shows wedge-shape consolidations located in lingular segment in left lung (black narrow arrow).

Patients characteristics are presented in [Table 3](#).

Invasive pulmonary aspergillosis was confirmed by positive galactomannan blood ($n = 35$) or BALF ($n = 2$) test.

All patients had abnormal findings in HRCT ([Table 4](#)).

In all patients typical findings of IPA occurred. In 11.4% wedge-shaped consolidations were seen without any other typical lesions.

In 21 patients (60%) we found coexisting atypical radiological lesions. GGO occurred in 31.4% and

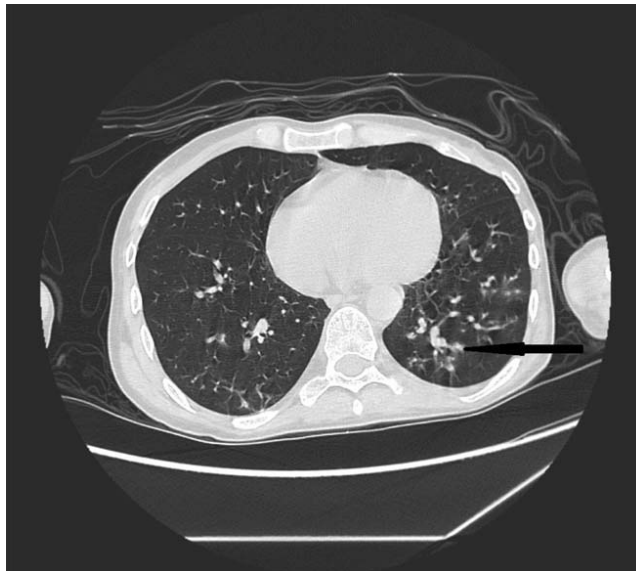


Figure 9. 37-year-old male with acute myeloid leukemia 26 days after bone marrow transplantation presenting with fever. High resolution CT scan obtained at level of lower lobes shows peripherally located nodules and micronodules with halo sign in left lower lobe (black narrow arrow).

pleural effusion occurred in 34.3% of patients. Enlarged lymph nodes occurred in 11.4%. None of the patients had the atypical lesions alone.

The most common HRCT findings in our study were nodules with halo (88.5%) and wedge shape consolidations (48.6%). None of the patients presented any air crescent signs or cavities.

In patients with micronodules which are considered to be typical lesions, concomitant atypical findings were observed in 57.1% ($p = 0.007$) (Table 5).

In patients with 10 or more lesions, the atypical pattern was dominant, and occurred in 48.6% ($p = 0.02$).

When lesions were located simultaneously centrally and peripherally, the atypical IPA features were coexisting in 62% of patients ($p = 0.08$).

In patients with 10 or more lesions, in 66.6% the distribution was both central and peripheral ($p < 0.001$) (Table 6).

Progression of the IPA was observed in the control HRCT in 10 patients (28.6%), the majority of this group (70%) consisted of patients with atypical IPA lesions. The early mortality rate, within three months after the baseline HRCT, was 25.7% and related to IPA progression. The overall mortality rate was 28.6%.

Discussion

The type of lesions considered typical for IPA has been expanding over time. Traditionally the most typical IPA findings were air-crescent signs and cavities [13]. With

Table 3. Patients characteristics.

Patients characteristics	
Sex(f/m)	11/24
Age: range, median	22–84, 65
Disease*	
AML	14
MM	6
ALL	3
MDS	2
AA	2
Other	8
alloHSCT	13
Progression of IPA**	10
Mortality***	9

*AML, acute myeloid leukemia; MM, multiple myeloma; ALL, acute lymphoblastic leukemia; MDS, myelodysplastic syndrome; AA, aplastic anemia.

**progression of radiologic findings in control HRCT after 2 weeks.

***early mortality within 3 months from the baseline HRCT.

Table 4. Characteristics of pulmonary findings.

HRCT findings	% (n = 35)*
Nodules with halo	88.5 (31)
Nodules	37.1 (13)
Wedge-shape or lobar consolidations	48.6 (17)
Ground glass opacities	31.4 (11)
Cavity	–
Air crescents sign	–
Pleural effusion	34.3 (12)
Septal thickening	14.3 (5)
Enlarges lymph nodes	11.4 (4)

*each patient could have more than one type of lesion.

Table 5. Location and number of lesions.

	Typical for IPA n (%)	Atypical for IPA n (%)	p-value
Location			
Central	1 (7)	1 (5)	1
Peripheral	9 (64)	7 (33)	0.09
C + P*	4 (28)	13 (62)	0.08
Number of lesions			
<10	7 (20)	4 (11.4)	0.72
≥10	7 (20)	17 (48.6)	0.02
Size of lesions (mm)**			
<10	8 (22.8)	20 (57.1)	0.007
10–50	8 (22.8)	10 (28.6)	0.79
>50	3 (8.6)	5 (14.2)	0.71

*central+ peripheral.

**each patient could have more than one type of lesion.

Table 6. Location of the lesions according to the number of lesions.

	<10	≥10	p-value
Central	2	0	0.49
Peripheral	8	8	1
C + P*	1	16	<0.001

*central + peripheral.

the advent of diagnostic methods currently they are regarded as late signs. In our study group, they were not observed in any of the patients.

Currently, the majority of patients are diagnosed early in the course of IPA and typical HRCT findings include nodules, nodules with halo and consolidations [14]. Interpretation of such findings must be always done in the context of patients' clinical symptoms and results of laboratory tests. All patients in our study group presented with typical findings. The diagnostic procedures in hematology patients should be guided by the underlying disease, leukocyte count and clinical symptoms [15].

According to the latest EORTC MSG criteria, the wedge shape, segmental or lobar consolidations were introduced as typical for IPA. This type of lesion occurred in 48.6% of our patients while 11.4% occurred as the only typical finding (see Table 4). Segmental, lobar or wedge-shaped consolidations occur in bacterial pneumonia or pulmonary infarction due to pulmonary embolism. Other conditions that should be considered in differential diagnosis include septic pulmonary emboli and pulmonary hemorrhage [16].

Nodules were found in 37.1% of patients (see Table 4). As the differential diagnosis of pulmonary nodules is broad, the occurrence of relevant symptoms, the number of nodules, and their imaging characteristics (location, shape, presence and type of calcifications, and presence of spiculation or cavitation) may narrow the differential diagnosis. Even though considered typical for IPA their size and number should be verified with previous HRCT whenever possible. Nodules can be the manifestation of previous pneumonias [17].

The halo sign is a well-known pattern of IPA [18]. In our study group, it occurred in 88.5% (see Table 4). The

sign itself is non-specific. Apart from infection-related condition, many neoplastic and inflammatory processes can cause halo sign. However, in the context of patients with hematological malignancies, it suggests IPA [19].

In the study group, 31.4% of patients had GGO (see Table 4). However, when overlapping typical and atypical findings are seen, especially GGO, mixed pneumonia etiology should be considered. In such cases, differential diagnosis should include viral lower respiratory tract infections and *Pneumocystis jiroveci* [20].

Pleural effusions were categorized as atypical findings. It occurred in 34.3% of patients, however, due to the older age of our study population and comorbidities the IPA etiology of pleural effusions is unlikely (see Table 4). Overall, fungal infections account for less than 1% of all pleural effusions [21].

Enlarged lymph nodes are a rare finding in IPA itself and this finding is reported in the literature occasionally, rather in case reports [22,23]. In our study group enlarged lymph nodes occurred in 11.4% (see Table 4).

Another atypical finding for IPA is septal thickening. This finding may be the manifestation of different entities, corresponding with the Kerley B lines seen on X-rays [24].

The major limitations of our study were retrospective data collection and a small study group. None of the patients in our study group had a histologically or culture proven IPA.

As the sensitivity of the serum testing is relatively low and radiologic signs of IPA have been shown to precede serum galactomannan testing [25], the HRCT is a major diagnostic tool.

It suggests that in the cases of hematological malignancies, neutropenia and symptoms of infection, occurring with consolidations in baseline HRCT, the differential diagnosis should consider IPA.

Conclusions

Wedge-shape consolidations may add useful information for the diagnosis of invasive pulmonary aspergillosis in patients with underline disease of hematological malignancies. Employment of the latest EORTC/MSG criteria increased diagnostic value of the baseline high resolution computed tomography in our study group by 11.4%.

Data availability

The database used to support the findings of this study is available from the corresponding author upon request.

Disclosure statement

No potential conflict of interest was reported by the author(s).

ORCID

Marta Halaburda-Rola  <http://orcid.org/0000-0001-7185-3156>

Tomasz Dzieciatkowski  <http://orcid.org/0000-0002-9983-1992>

Olgierd Rowiński  <http://orcid.org/0000-0001-9519-0668>

Laretta Grabowska-Derlatka  <http://orcid.org/0000-0002-6511-6579>

References

- [1] Vazquez JA, Tovar-Torres MP, Hingwe A, et al. The changing epidemiology of invasive aspergillosis in the non-traditional host: risk factors and outcomes. *Pulm Crit Care Med.* 2016;1(3):67–71.
- [2] Cornet M, Fleury L, Maslo C, et al. Epidemiology of invasive aspergillosis in France: a six-year multicentric survey in the Greater Paris area. *J Hosp Infect.* 2002;51:288–296.
- [3] Barnes PD, Marr KA. Risks, diagnosis and outcomes of invasive fungal infections in haematopoietic stem cell transplant recipients. *Br J Haematol.* 2007;139:519–531.
- [4] Baddley JW. Clinical risk factors for invasive aspergillosis. *Med Mycol.* 2011;49(Suppl 1):S7–S12.
- [5] Marr KA, Carter RA, Boeckh M, et al. Invasive aspergillosis in allogeneic stem cell transplant recipients: changes in epidemiology and risk factors. *Blood.* 2002;100(13):4358–4366.
- [6] Kousha M. Pulmonary aspergillosis: a clinical review. *Eur Respir Rev.* 2011;20(121):156–174.
- [7] Young AY, LeivaJuarez MM, Evans SE. Fungal pneumonia in patients with hematologic malignancy and hematopoietic stem cell transplantation. *Clin Chest Med.* 2017;38(3):479–491.
- [8] Donnelly JP, Chen SC, Kauffman CA, et al. Revision and update of the consensus definitions of invasive fungal disease from the European Organization for Research and Treatment of Cancer and the Mycoses Study Group Education and Research Consortium. *Clin Infect Dis.* 2020;71(6):1367–1376.
- [9] Michallet M, Bénét T, Sobh M, et al. Invasive aspergillosis: an important risk factor on the short- and long-term survival of acute myeloid leukemia (AML) patients. *Eur J Clin Microbiol Infect Dis.* 2012;31:991–997.
- [10] Cattaneo C, Gramegna D, Malagola M, et al. Invasive pulmonary aspergillosis in acute leukemia: a still frequent condition with a negative impact on the overall treatment outcome. *Leuk Lymphoma.* 2019;60(12):3044–3050.
- [11] Patterson TF, Thompson GR, Denning DW, et al. Practice guidelines for the diagnosis and management of aspergillosis: 2016 update by the Infectious Diseases Society of America. *Clin Infect Dis.* 2016;63:e1–e60.
- [12] Austin JH, Muller NL, Friedman PJ, et al. Glossary of terms for CT of the lungs: recommendations of the Nomenclature Committee of the Fleischner Society. *Radiology.* 1996;200:327–331.
- [13] Brodoefel H, Vogel M, Hebart H, et al. Long-term CT follow-up in 40 non-HIV immunocompromised patients with invasive pulmonary aspergillosis: kinetics of CT morphology and correlation with clinical findings and outcome. *Am J Roentgenol.* 2006;187(2):404–413.
- [14] Greene RE, Schlamm HT, Oestmann JW, et al. Imaging findings in acute invasive pulmonary aspergillosis: clinical significance of the halo sign. *Clin Infect Dis.* 2007;44:373–379.

- [15] Bergeron A, Porcher R, Sulahian A, et al. The strategy for the diagnosis of invasive pulmonary aspergillosis should depend on both the underlying condition and the leukocyte count of patients with hematologic malignancies. *Blood*. 2012;119(8):1831–1837.
- [16] He H, Stein MW, Zalta B, et al. Pulmonary infarction: spectrum of findings on multidetector helical CT. *J Thorac Imaging*. 2006;21:1–7.
- [17] Loverdos K, Fotiadis A, Kontogianni C, et al. Lung nodules: a comprehensive review on current approach and management. *Ann Thorac Med*. 2019;14(4):226–238.
- [18] Kuhlman JE, Fishman EK, Siegelman SS. Invasive pulmonary aspergillosis in acute leukemia: characteristic findings on CT, the CT halo sign, and the role of CT in early diagnosis. *Radiology*. 1985;157:611–614.
- [19] Lee YR, Choi YW, Lee KJ, et al. CT halo sign: the spectrum of pulmonary diseases. *Brit J Radiol*. 2005;78:862–865.
- [20] Magira EE, Chemaly RF, Jiang Y, et al. Outcomes in invasive pulmonary aspergillosis infections by respiratory viral infections in patients with hematologic malignancies: a case control study. *Open Forum Infect Dis*. 2019;6(7):ofz247.
- [21] Light RW. *Pleural disease*, Vol. 11. 4th ed. Baltimore: Williams and Wilkins; 2001; Pleural effusion secondary to fungal infections, actinomycosis, and nocardiosis. p. 196–203.
- [22] Nourbakhsh E, Goodman S, Nugent K, et al. Generalized lymphadenopathy secondary to an invasive fungal infection in an apparently healthy patient. *Am J Med Sci*. 2010;340(1):84–88.
- [23] Su SS, Zhou Y, Xu H-Y, et al. Invasive aspergillosis presenting as hilar masses with stenosis of bronchus: a case report. *World J Clin Cases*. 2019;7(22):3832–3837.
- [24] Collins J. CT signs and patterns of lung disease. *Radiol Clin North Am*. 2001;39(6):1115–1135.
- [25] Weisser M, Rausch C, Droll A, et al. Galactomannan does not precede major signs on a pulmonary computerised tomographic scan suggestive of invasive aspergillosis in patients with hematologic malignancies. *Clin Infect Dis*. 2005;41:1143–1149.

Article

Comparison of Computed Tomography Scoring Systems in Patients with COVID-19 and Hematological Malignancies

Marta Hałaburda-Rola ^{1,*}, Joanna Drozd-Sokołowska ², Magdalena Januszewicz ¹ and Laretta Grabowska-Derlatka ¹¹ Hind Department of Clinical Radiology, Medical University of Warsaw, 01-445 Warsaw, Poland² Department of Hematology, Transplantation and Internal Diseases, Medical University of Warsaw, 01-445 Warsaw, Poland

* Correspondence: mrola@wum.edu.pl

Simple Summary: COVID-19 pneumonia poses a serious threat in hematologic patients. Computed tomography is an indispensable tool supporting diagnosis. A better and more objective analysis of the extent of pneumonia enables assessment of the extent of the disease as well as the selection of prognostic factors of death. The aim of this study is to compare four different computed tomography scoring systems (three semiquantitative and one qualitative) in hematology patients to better select patients at risk of death and choose the scoring system that is the most feasible for this group of patients.

Abstract: Background: Numerous computed tomography (CT) scales have been proposed to assess lung involvement in COVID-19 pneumonia as well as correlate radiological findings with patient outcomes. Objective: Comparison of different CT scoring systems in terms of time consumption and diagnostic performance in patients with hematological malignancies and COVID-19 infection. Materials and methods: Retrospective analysis included hematological patients with COVID-19 and CT performed within 10 days of diagnosis of infection. CT scans were analyzed in three different semi-quantitative scoring systems, Chest CT Severity Score (CT-SS), Chest CT Score (CT-S), and Total Severity Score (TSS), as well as qualitative modified Total Severity Score (m-TSS). Time consumption and diagnostic performance were analyzed. Results: Fifty hematological patients were included. Based on the ICC values, excellent inter-observer reliability was found among the three semi-quantitative methods with ICC > 0.9 ($p < 0.001$). The inter-observer concordance was at the level of perfect agreement (kappa value = 1) for the mTSS method ($p < 0.001$). The three-receiver operating characteristic (ROC) curves revealed excellent and very good diagnostic accuracy for the three quantitative scoring systems. The AUC values were excellent (0.902), very good (0.899), and very good (0.881) in the CT-SS, CT-S and TSS scoring systems, respectively. Sensitivity showed high levels at 72.7%, 75%, and 65.9%, respectively, and specificity was recorded at 98.2%, 100%, 94.6% for the CT-SS, CT-S, and TSS scoring systems, respectively. Time consumption was the same for Chest CT Severity Score and TSS and was longer for Chest CT Score ($p < 0.001$). Conclusions: Chest CT score and chest CT severity score have very high sensitivity and specificity in terms of diagnostic accuracy. The highest AUC values and the shortest median time of analysis in chest CT severity score indicate this method as preferred for semi-quantitative assessment of chest CT in hematological patients with COVID-19.

Keywords: COVID-19; computed tomography; hematological malignancies; pneumonia; imaging

Citation: Hałaburda-Rola, M.; Drozd Sokołowska, J.; Januszewicz, M.; Grabowska-Derlatka, L. Comparison of Computed Tomography Scoring Systems in Patients with COVID-19 and Hematological Malignancies. *Cancers* **2023**, *15*, 2417. <https://doi.org/10.3390/cancers15092417>

Academic Editor: Mingyi Chen

Received: 26 February 2023

Revised: 16 April 2023

Accepted: 21 April 2023

Published: 22 April 2023



Copyright: © 2023 by the authors. Licensee MDPI, Basel, Switzerland. This article is an open access article distributed under the terms and conditions of the Creative Commons Attribution (CC BY) license (<https://creativecommons.org/licenses/by/4.0/>).

1. Introduction

In December 2019, the COVID-19 pandemic, caused by severe acute respiratory syndrome coronavirus 2 (SARS-CoV-2), began in Wuhan, China, and spread worldwide, especially affecting the elderly and those with comorbidities [1]. In patients with hematological malignancies, COVID-19 caused a high mortality rate and often required

withdrawal of anticancer treatment [2]. The pandemic has forced healthcare providers to develop dedicated diagnostic procedures. The primary method of diagnosing SARS-CoV-2 virus infection is real-time reverse transcription polymerase chain reaction (RT-PCR) or next-generation sequencing from nasopharyngeal swabs. Imaging techniques are considered additional diagnostic methods performed depending on the severity of clinical symptoms. Chest X-ray has been proven to have no predictive value in patients with COVID-19, as it can give false negatives in patients with mild symptoms [3]. However, in patients admitted to an intensive care unit (ICU), who require oxygen support, mechanical ventilation, sedation, and are in severe clinical conditions, a portable chest X-ray remains an indispensable basic imaging tool [4]. Computed tomography (CT) shows high sensitivity in the diagnosis of suspected COVID-19 and is used to guide patient management [5]. According to the Polish Medical Society of Radiology, the main indications for chest CT are a high risk of progression of COVID-19 or development of its complications. As long as the pulmonary embolism is not suspected, contrast administration is not routinely recommended [4].

Chest CT findings in COVID-19 pneumonia are nonspecific and resemble those in other viral pneumonias, usually presenting as bilateral areas of ground glass opacities (GGO) and consolidations located predominantly peripherally, bilaterally in the lower lobes. Superimposed thickening of the interlobular septum results in a “crazy-paving” appearance. In severe cases, patients present radiological features of acute respiratory distress syndrome (ARDS) [6].

Patients with hematologic diseases usually present with immune deficiencies, including neutropenia either due to the hematological condition itself or anticancer therapy.

Thus, there are often infectious complications and superinfections of the diseases themselves and treatment. Chest CT is an indispensable tool in these cases to assess lung involvement in COVID-19 pneumonia and to evaluate any possible concomitant abnormalities such as nodules with halos or other features suggestive of invasive fungal infections or other pathologies. Chest CT provides an opportunity to objectively assess the degree of lung involvement in patients with COVID-19. Several scales have been developed to evaluate the lesions and enable more objective semi-quantitative and qualitative analysis.

There are a few papers describing the challenges and pitfalls of chest CT imaging in hematologic patients, but there is a lack of information on quantitative CT analysis in this particular group of patients [7]. The aim of this study was to compare the sensitivity and specificity of three semiquantitative CT scoring systems in terms of diagnostic accuracy and time-consumption in patients with hematologic diseases and COVID-19 and interobserver agreement in the qualitative analysis of lung parenchyma.

2. Materials and Methods

2.1. Study Design and Patient Population

This single-center, retrospective study includes 50 consecutive patients with hematological diseases and positive RT-PCR test results for COVID-19, diagnosed between March 2020 and October 2021.

The severity of COVID-19 was assessed according to the recommendations of the Polish Association of Epidemiologists and Infectiologists [8]. According to this classification, stage 1 is asymptomatic or mildly symptomatic, with oxygen saturation as measured by pulse oximetry (SpO₂) of $\geq 94\%$. In stage 1, patients do not require hospitalization because of COVID-19. Stage 2 is fully symptomatic, with SpO₂ < 94% and the requirement for hospitalization because of the need for oxygen therapy. Stage 3 is defined as respiratory failure with SpO₂ < 90% and requirement for high-flow oxygen therapy. Stage 4 is defined as ARDS with the need for invasive mechanical ventilation (IMV) and ICU treatment. Stages 1 and 2 were considered as the non-severe COVID-19 group, while stage 3 and 4 were considered as the severe COVID-19 group. The indications for CT were mild,

non-specific symptoms of respiratory tract infection and clinical risk factors for developing complications. CT was performed immediately after a positive SARS-CoV-2 RT-PCR test. Comorbidities, complete blood count parameters, laboratory parameters such as D-dimer, and C-reactive protein (CRP) at the time of admission diagnosis were recorded.

2.2. Chest Computed Tomography

The CT scans were obtained on supine position at the end-inspiratory effort using a GE 64-row scanner. The thoracic scanning parameters were as follows: tube voltage of 120 kV, tube current of 240–460 mA, 1.25 mm collimation, a pitch of 0.984:1, and applying a large field of view and a rotation time of 0.7 s. From this dataset, axial slices of 1 mm were obtained. The coronal and sagittal slices were obtained as high resolution multiplanar reformation images. All CT exams were obtained without intravenous contrast administration. Images were analyzed using picture archiving and communications systems (PACS).

The CT evaluation was performed by two independent, board-certified radiologists. Each observer analyzed the examination in four scales. Time consumption on reporting of each patient scoring system was recorded and calculated in the same reading environment using the same diagnostic monitors.

The software used for the image analysis was GE AW Server 3.2 ext. 4.0.

According to Fleischner Society, a standard glossary of terms for computed tomography was applied to describe the lesions [9]:

- GGO was defined as hazy increased attenuation of lung with preserved bronchial and vascular margins;
- Consolidation was considered an increase in pulmonary parenchymal attenuation that obscures the airways and vessels;
- Crazy paving was the area of GGO with coexisting thickening of interlobular septae;
- Pleural effusion was described as a free fluid in the pleural cavity;
- Septal thickening comprised abnormal widening of an interlobular septum or septae;
- Subpleural lines comprised a thin curvilinear opacity of a few millimeters or less thickness usually less than 1 cm from pleural surface and paralleling the pleura.

The chest CT exams were evaluated according to four scoring systems described below:

- Chest CT Severity Score (CT-SS): According to the anatomic structure, the 18 segments of both lungs were divided into 20 regions, in which the posterior apical segment of the left upper lobe was subdivided into apical and posterior segmental regions, whereas the anteromedial basal segment of the left lower lobe was subdivided into anterior and basal segmental regions. The lung opacities in all of the 20 lung regions were subjectively evaluated on chest CT images using a system attributing score of 0, 1, and 2 if parenchymal opacification involved 0%, less than 50%, or equal to or more than 50% of each region, respectively. The CT-SS was defined as the sum of the individual scores in the 20 lung segment regions, which may range from 0 to 40 points [6];
- Chest CT Score (CT-S): Each of the five lung lobes was visually scored on a scale of 0 to 5, with 0 indicating no involvement; 1, less than 5% involvement; 2, 5–25% involvement; 3, 26–49% involvement; 4, 50–75% involvement; and 5, more than 75% involvement. The total CT score was the sum of the individual lobar scores and ranged from 0 (no involvement) to 25 (maximum involvement) [10,11];
- Total severity score (TSS): The TSS was calculated for each of the 5 lobes in all patients. According to the extent of pulmonary involvement, each lobe could be scored from 0 to 4 points as the following: 0, no involvement; 1, from 1 to 25% involvement; 2, from 26 to 50% involvement; 3, from 51 to 75% involvement; and 4, more than 75% involvement. The sum of each individual lobar score resulted in the TSS, which ranged from 0 to 20 [12];

- Modified Total Severity Score (m-TSS): m-TSS scale includes additional qualitative features of lung involvement: A–ground glass opacity, B–crazy-paving pattern, C–consolidations, and X–character other than enlisted [13].

2.3. Viral Analysis

Nasopharyngeal swab analysis was performed in each patient at admission to the hospital and afterward in patients with clinical symptoms of viral infection or in patients with known contact with SARS-CoV2-infected patients.

The diagnosis of SARS-CoV-2 infection was based on a nucleic acid amplification test (Seegene STARlet®, Bio-Rad CFX®, Hologic Panther®, Warsaw, Poland) using nasopharyngeal swabs.

2.4. Statistical Analysis

The MS Power BI Desktop was applied for finding the outliers via scatter chart in the first phase of the analysis and preliminary statistical analysis. IBM SPSS Statistics (version: 28.0.1.0(142)) was used to analyze the distribution of variables and perform some statistical tests and calculate some statistics. PQStat (version: 1.8.4.) was used for the same purpose to analyze the data and to prepare all the visualizations seen in this article. To determine the inter-observer agreement between the two reviewers, two tests were used. The Kaplan–Meier curve was used to calculate the median overall survival time for ICU cases and PCR test cases. To check the significance of the nominal variables, the test of kappa coefficient was applied. Whereas for the interval variables (after checking and confirming the normal distribution with an appropriate statistical test) a test to check the significance of the ICC coefficient (intraclass correlation coefficient) was used. Intraclass correlation (ICC) was used to examine inter-observer agreement for the three quantitative methods (CT-SS, CT-S, and TSS). The determination of the ROC curve and the calculation of the area under this curve (AUC), as well as the calculation of sensitivity and specificity, were used to compare which of the 3 quantitative methods could generate the best results in assigning patients to the severe and non-severe COVID-19 groups. After comparing the three quantitative methods, i.e., CT-SS, CT-S, and TSS, in terms of inter-observer agreement and in terms of ROC curve, AUC, and sensitivity and specificity values, the time consumptions of the three test methods were compared. For this purpose, the normal distribution of the three variables was checked. When the test showed that one of the variables did not meet the condition of normal distribution (p -value > 0.05) it was decided to perform Friedman’s ANOVA test, which was dedicated to the independent interval variable that did not meet the condition of normal distribution. Patients were divided into two groups: the severe COVID-19 group and non-severe COVID-19 group. To determine the p -value, three different tests were used. The main aim was to define whether the p -value was less than 0.05, indicating a statistically significant difference. For interval scale variables that did not meet the condition of normal distribution and for those that were independent, the Mann–Whitney U test was used, which is specifically designed for such conditions. For quantitative variables that met the condition of normal distribution, the Student’s t -test for independent groups was used. For nominal and independent variables, the chi-square/Fisher’s exact test was used. In order to compare the time consumption of the three semi-quantitative methods of assessing patients’ lungs (Chest CT severity score_time, Chest CT score_time, and Total severity score_time), the normal distribution of these variables was checked at first. Due to the small sample size, the Shapiro–Wilk test was used to test the normal distribution condition of the variables describing the examination/interpretation time in seconds. According to the null hypothesis of the Shapiro–Wilk test, the distribution of the trait under study is a normal distribution. Thus, if the p -value was less than the chosen α level ($\alpha = 0.05$ in this study), the null hypothesis was rejected, and there was evidence that the values did not have a normal distribution. The p -value for this test for the Chest CT severity score time variable was <0.005 , i.e., the Chest CT severity score_time variable did not meet the normal distribution condition, whereas

the other two variables met the normal distribution condition. For this reason, it was not possible to carry out the test that was previously considered, that is, the single-factor repeated-measures ANOVA test. Instead of the previously considered test, the Friedman ANOVA test, which is dedicated to dependent interval variables meeting the condition of normal distribution, was conducted. Friedman's ANOVA test for p -value < 0.005 indicates that not all test times are statistically significantly different from each other.

3. Results

50 patients with hematologic malignancies and COVID-19 diagnosed at the Medical University of Warsaw were included in this study. The clinical data of the patients are presented in Table 1.

Table 1. Clinical and radiological characteristics of the studied patients according to COVID-19 disease progression.

Characteristic	Total	Non-Severe COVID-19	Severe COVID-19	p Value
N	50	28	22	
Age [years]	64.94 ± 17.45	61.32 ± 18.53	69.55 ± 15.16	0.096 ^U
Sex				0.136 ^F
Male	33 (66%)	16 (57.14%)	17 (77.27%)	
Female	17 (34%)	12 (42.86%)	5 (22.73%)	
Mortality rate	20 (40%)	1 (3.57%)	19 (86.36%)	<0.05 ^F
Associated comorbidities	1.92 ± 1.44	1.61 ± 1.2	2.32 ± 1.64	0.1097 ^U
Arterial hypertension	26 (52%)	12 (42.86%)	14 (63.64%)	0.144 ^F
Diabetes	9 (18%)	2 (7.14%)	7 (31.82%)	0.024 ^F
Liver disease	5 (10%)	2 (7.14%)	3 (13.64%)	0.447 ^F
Hyperlipidemia	18 (36%)	9 (32.14%)	9 (40.91%)	0.522 ^F
Heart disease	23 (46%)	14 (50%)	9 (40.91%)	0.522 ^F
Kidney disease	15 (30%)	6 (21.43%)	9 (40.91%)	0.136 ^F
Blood pressure				
Systolic pressure [mmHg]	120.22 ± 18.64	118.86 ± 16.19	121.95 ± 21.64	0.565 ^t
Systolic blood pressure out of the norm	4 (8%)	2 (7.14%)	2 (9.09%)	0.801 ^F
Diastolic pressure [mmHg]	71.16 ± 11.14	72.25 ± 10.51	69.77 ± 12	0.441 ^t
Diastolic blood pressure out of the norm	4 (8%)	2 (7.14%)	2 (9.09%)	0.801 ^F
Admitted to ICU	19 (38%)	3 (10.71%)	16 (72.73%)	<0.05 ^F
Ventilated by a mask with high oxygen volumes	21 (42%)	2 (7.14%)	19 (86.36%)	<0.05 ^F
Intubated	13 (26%)	1 (3.57%)	12 (54.55%)	<0.05 ^F
Saturation [%]	89.04 ± 13.72	94.11 ± 7.96	82.59 ± 16.72	0.001 ^U
D-dimer [ug/L]	2882.42 ± 2771.56	2348.39 ± 2836.64	3562.09 ± 2591.12	0.005 ^U
CRP, C Reactive Protein [mg/l]	141.58 ± 86.98	111.04 ± 79.96	180.45 ± 81.27	0.004 ^t
WBC, White blood cell count [tys/mm ³]	8.69 ± 11.34	9 ± 11.8	8.3 ± 10.99	0.71032 ^U
Neutrophil [tys/uL]	3.9516 ± 5.79	5.17 ± 7.21	2.4 ± 2.61	0.186734 ^U

Test of significance: ^U the Mann-Whitney U test, ^F chi-square or Fisher's exact test, ^t independent samples t test.

3.1. Clinical and Radiological Characteristics of the Examined Patients According to COVID-19 Severity

In the study sample of patients, 22 (56%) were severe cases, and 28 (44%) belonged to the non-severe COVID-19 group. During the analysis, a statistically significant difference was noted between the mortality rates of severe and non-severe COVID-19 patients. The Severe COVID-19 group had a mortality rate of 86.36%, while there was only one case of death in the non-severe group, resulting in a mortality rate of 3.57% (p -value < 0.05).

Compared to the non-severe COVID-19 group, patients in the severe COVID-19 group were more likely to demonstrate the presence of a comorbid condition, such as diabetes. Among severely ill COVID-19 patients, 16 (72.73%) were admitted to the ICU, while among non-severe patients, only 3 (10.71%) were admitted to the ICU (p -value < 0.05).

Saturation levels were statistically different between the two groups of patients (Figure 1). The mean saturation level in non-severe patients oscillated at 94.11% (SD 7.96), whereas for severe patients, this value was 82.59% (SD 16.72) (p -value = 0.001). The D-dimer value differed significantly in the groups designated for analysis (Figure 2) between severely ill patients (mean D-dimer 3562.09 ug/L; SD 2591.12) and non-severe patients (mean D-dimer 2348.39 ug/L; SD 2836.64, p -value = 0.005). The blood-based CRP value (Figure 3) was also higher in severely ill COVID-19 patients (mean CRP 180.45 mg/L; SD 81.27) and non-severe patients (mean CRP 111.04 mg/L; SD 79.96, p -value = 0.004).

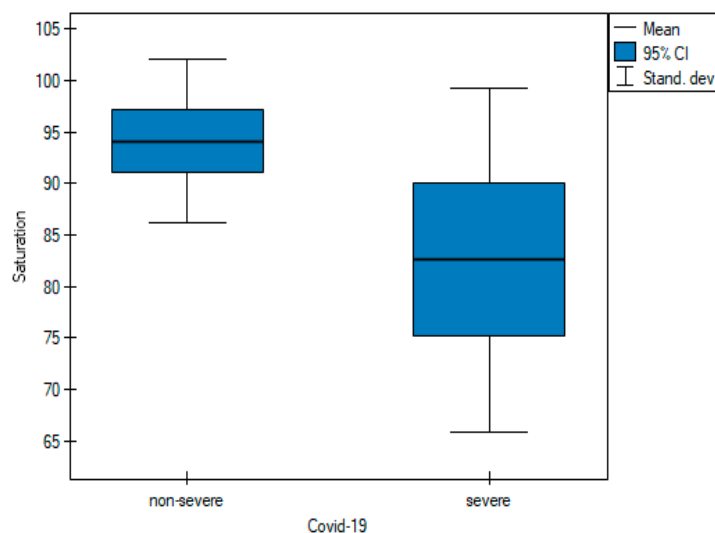


Figure 1. Pairwise comparisons of saturation values of non-severe and severe cases at diagnosis.

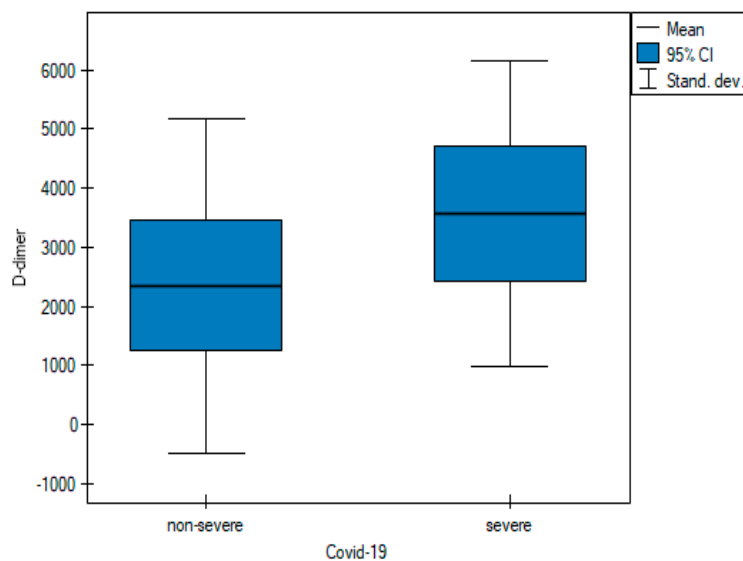


Figure 2. Pairwise comparisons of D-dimer values of non-severe and severe cases at diagnosis.

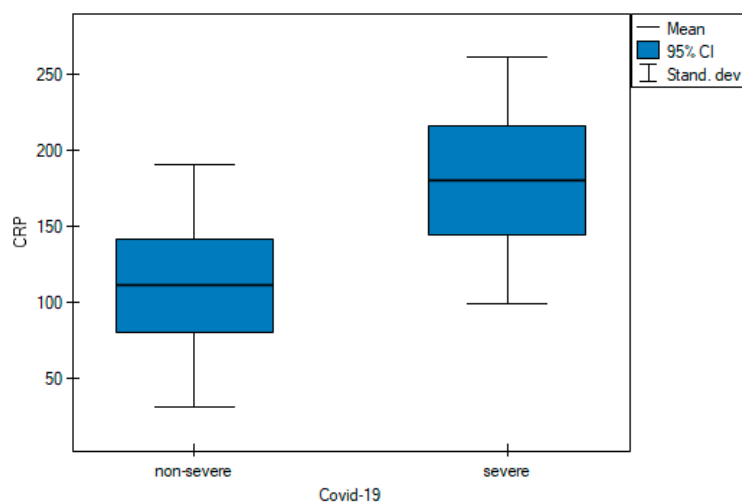


Figure 3. Pairwise comparisons of CRP values of non-severe and severe cases at diagnosis.

The Kaplan–Meier curve was used to determine a curve showing the probability of survival time for the patients from the time of admission to the ICU ($N = 19$), assuming a maximum time in hospital of 15 days. The premise of this analysis was to determine the median time to death after admission to the ICU and to show by means of a curve how the probability of survival time was distributed among the patients studied. While analyzing the Kaplan–Meier curve, it was observed that the median survival from ICU admission was 11 days, with a mean value of slightly over 9 days (Figure 4).

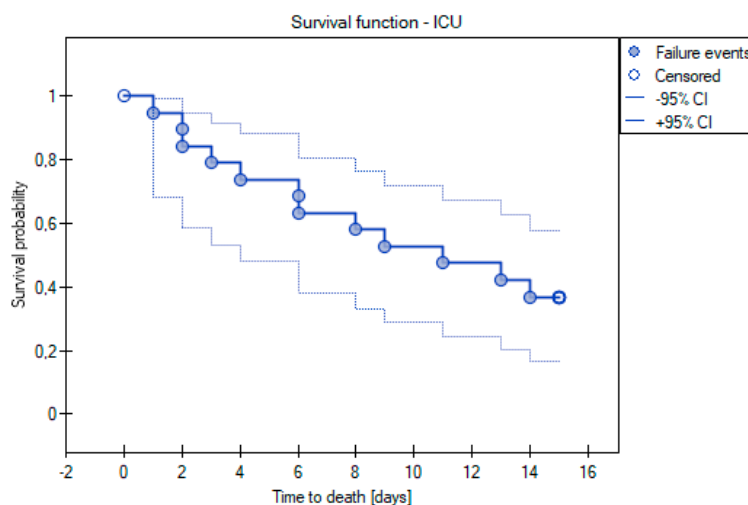


Figure 4. Kaplan–Meier curve for survival time analysis for ICU cases.

By using the Kaplan–Meier curve, we also decided to examine the median survival time of the patients using the PCR test. Kaplan–Meier curves were applied to examine the median survival time of the patients using the PCR test. Only the patients who died within 2 months of the PCR test were included in this analysis. Based on this curve, a median value of 10 days and a mean value of 14 days were determined (Figure 5).

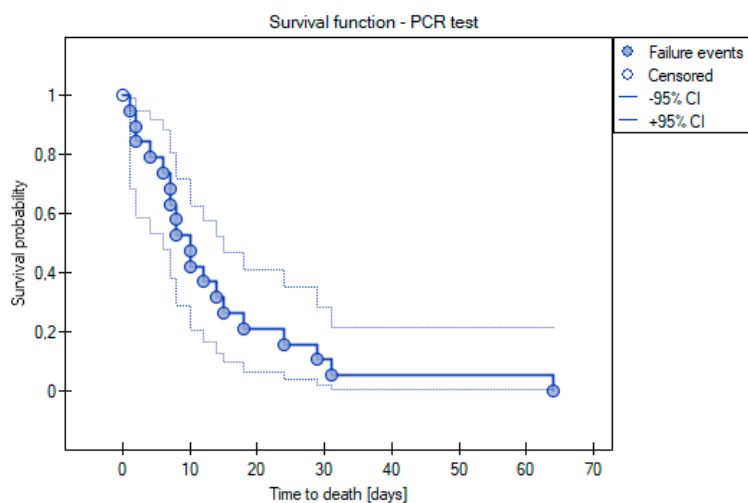


Figure 5. Kaplan–Meier curve for survival time analysis for PCR test cases.

3.2. Inter-Observer Agreement

For each scoring system, 100 observations were submitted.

There was statistically significant inter-observer agreement between the two observers in assessing qualitative lung involvement using the m-TSS method. The inter-observer

concordance oscillated at the level of perfect agreement (kappa value = 1) for four categories, i.e., GGO, crazy paving, consolidations, and normal lungs (Table 2).

Table 2. Test of significance: Fleiss' kappa for qualitative lung assessment via m-TSS performed by the two observers.

Category	Fleiss' Kappa (κ)	95% CI	SE	p Value
Overall	1	0.796–1	0.104	<0.001
Nomal lungs	1	0.723–1	0.141	<0.001
Ground glass opacities	1	0.723–1	0.141	<0.001
Crazy paving	1	0.723–1	0.141	<0.001
Consolidations	1	0.723–1	0.141	<0.001

κ —kappa value, CI—Confidence interval, SE—standard error.

As part of the inter-observer agreement analysis, an error plot was determined for the two observers (Figure 6), which graphically shows the same values shown in Table 2.

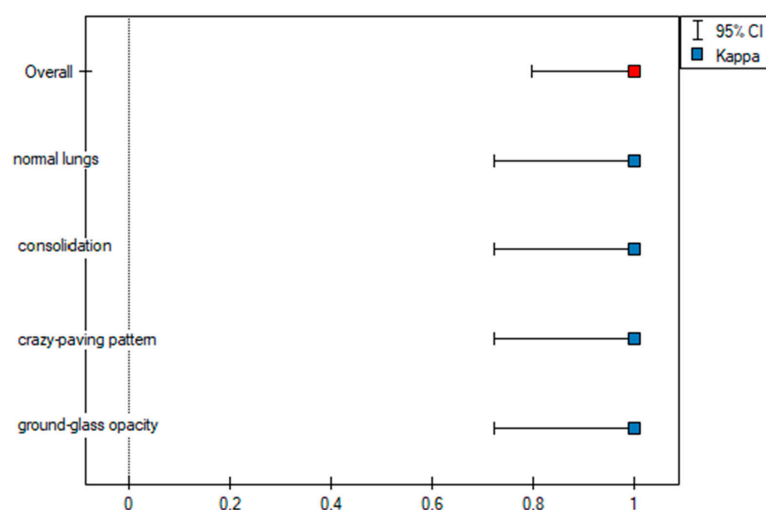


Figure 6. Error plot for the m-TSS method.

In addition, an agreement plot (Figure 7) was determined, which shows how the patient from the first to the fiftieth was rated by the two observers, where their agreement was 100%, which is why each column in the plot is the same color.

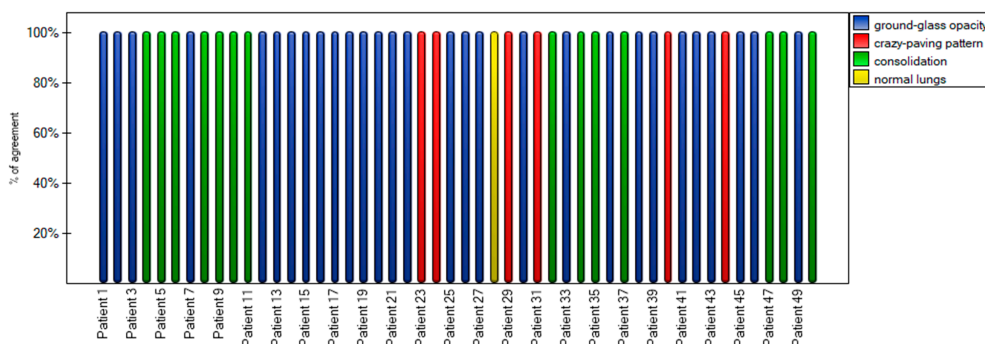


Figure 7. Agreement stacked column plot for the m-TSS method.

Based on the ICC values, excellent inter-observer reliability was found among the three methods, where ICC > 0.9 (Table 3).

Table 3. Inter-rater reliability for quantitative scoring systems.

Scoring System	ICC	95% CI	p Value
Chest CT severity score	0.994	0.99–0.997	<0.001
Chest CT score	0.994	0.99–0.997	<0.001
Total severity score	0.992	0.987–0.996	<0.001

ICC—Intraclass correlation coefficient, CI—Confidence interval.

To graphically represent the inter-observer agreement between the two observers in the quantitative methods shown in Table 3, multiple dot graphs were created (Figures 8–10).

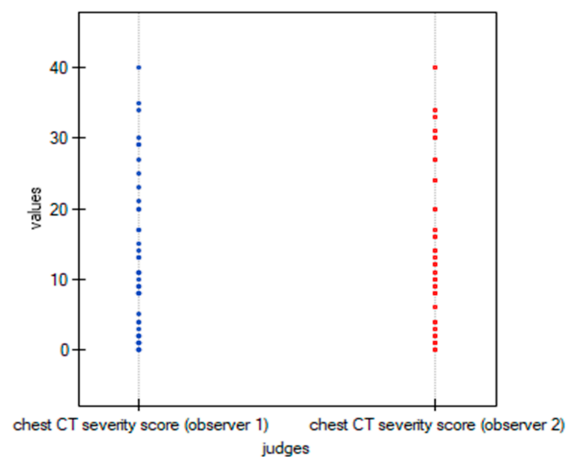


Figure 8. Multiple dot graphs for inter-observer agreement for Chest CT-SS.

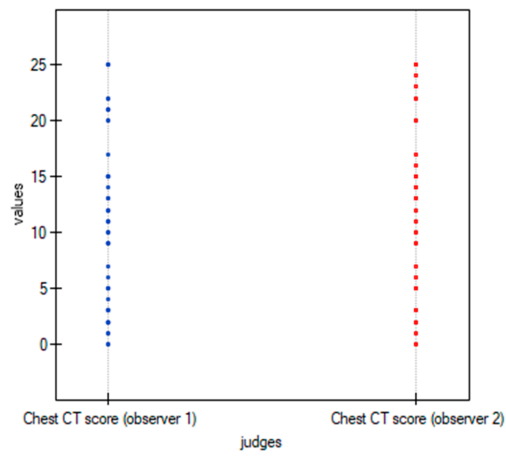


Figure 9. Multiple dot graphs for inter-observer agreement for Chest CT-S.

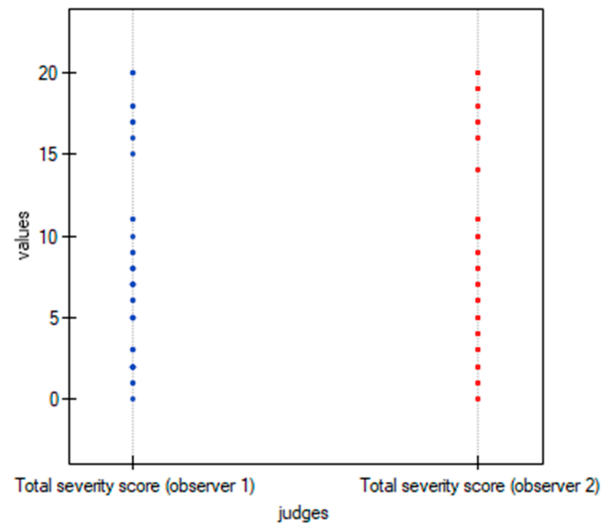


Figure 10. Multiple dot graphs for inter-observer agreement for TSS.

3.3. Severity Scoring Systems

The ROC curve was used to determine which of the three quantitative methods would best assign patients to the two groups according to the severity of COVID-19 disease. The two groups were determined: non-severe and severe, as described in the Materials and Methods section.

Table 4 shows all the values important for the comparison and analysis regarding the ROC curve for the three quantitative methods, i.e., range of values, sensitivity, specificity, cutoff value, AUC value, and *p*-value.

Table 4. Sensitivity and specificity of the quantitative methods for identifying the probability of COVID-19 adverse outcomes in the studied patients (severe and non-severe). The results were obtained based on the analysis of the ROC curves.

Scoring System	Range	Sensitivity	Specificity	Cutoff Value	AUC	p Value
Chest CT severity score	0–40	72.7%	98.2%	≥14	0.902	<0.001
Chest CT score	0–25	75%	100%	≥14	0.899	<0.001
Total severity score	0–20	65.9%	94.6%	≥9	0.881	<0.001

By using ROC curves (Figures 11–13), a selection of the optimal cutoff value was made, i.e., a certain value of the diagnostic variable that best divides the study population into two groups: severe and non-severe COVID-19. Comparing the results obtained for the ROC curves, it can be seen that for the two quantitative methods (Chest CT-SS and Chest CT-S), the cutoff value is the same at ≥ 14 , and for the TSS method it is ≥ 9 .

The three ROC curves revealed excellent and very good diagnostic accuracy for the three scoring systems. The AUC values were excellent (0.902), very good (0.899), and very good (0.881) for the CT-SS, CT-S, and TSS scoring systems, respectively. Sensitivity showed high levels at 72.7%, 75%, and 65.9% respectively, and specificity was recorded at 98.2%, 100%, and 94.6% for the CT-SS, CT-S, and TSS scoring systems, respectively.

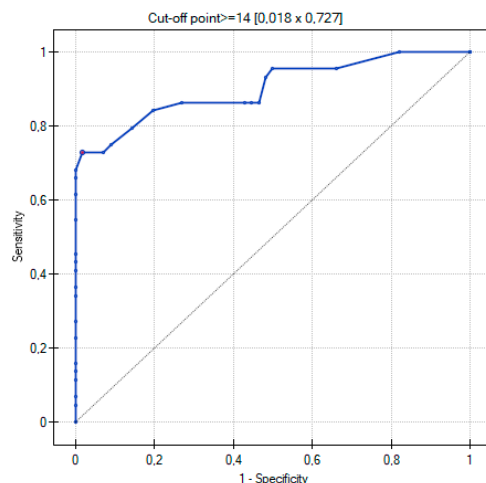


Figure 11. ROC curve for the diagnostic performance of Chest CT-SS in detection of severe COVID-19 cases.

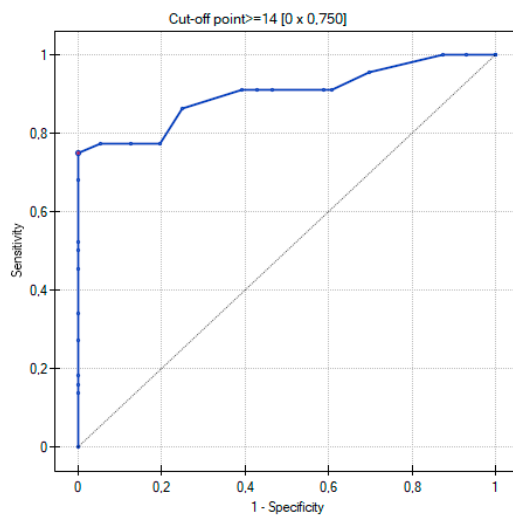


Figure 12. ROC curve for the diagnostic performance of Chest CT-S in detection of severe COVID-19 cases.

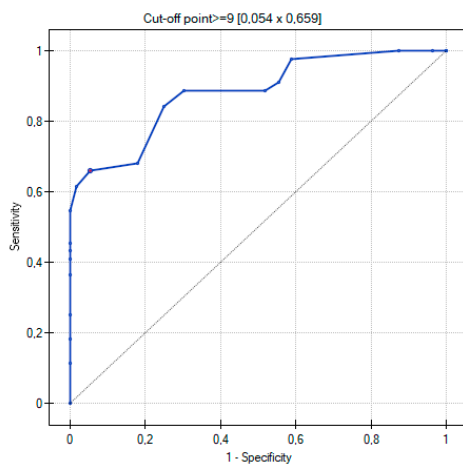


Figure 13. ROC curve for the diagnostic performance of TSS in detection of severe COVID-19 cases.

In order to be able to compare the mean values obtained when the two observers performed the three scoring methods for severe and non-severe COVID-19, a *t*-test for independent samples was performed. With the obtained *p*-value < 0.05 , box plots (Figures 14–16) were created to graphically visualize the obtained results. The same results are also presented in Table 5.

Table 5. The mean values of the three quantitative methods obtained with the tests conducted by the two observers.

Characteristic	Total	Non-Severe COVID-19	Severe COVID-19	p Value
Chest CT severity score	11.6 ± 10.78	5.02 ± 4.53	19.98 ± 10.64	<0.05 †
Chest CT score	10.62 ± 7.49	6 ± 4.15	16.5 ± 6.63	<0.05 †
Total severity score	7.74 ± 5.81	4.3 ± 2.68	12.11 ± 5.8	<0.05 †

Test of significance: t independent-samples t test.

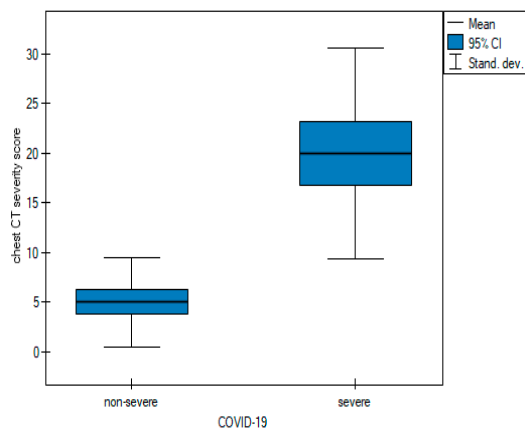


Figure 14. Box plot of comparisons of mean chest CT-SS for non-severe and severe COVID-19 patients.

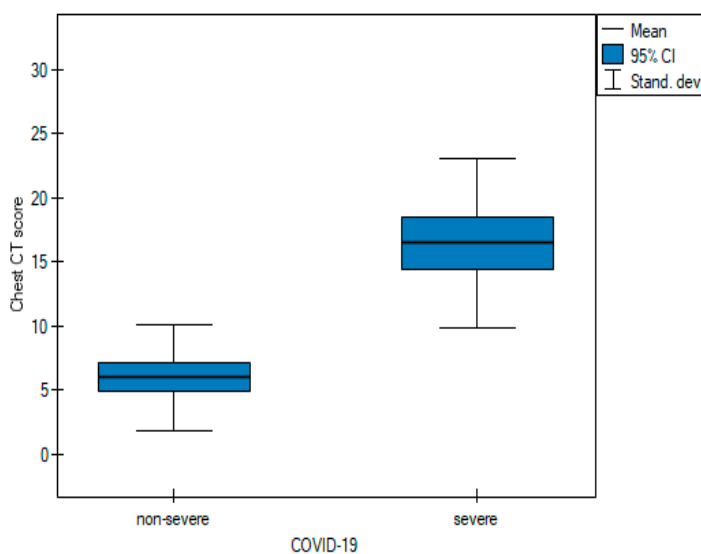


Figure 15. Box plot of comparisons of mean Chest CT-S for non-severe and severe COVID-19 patients.

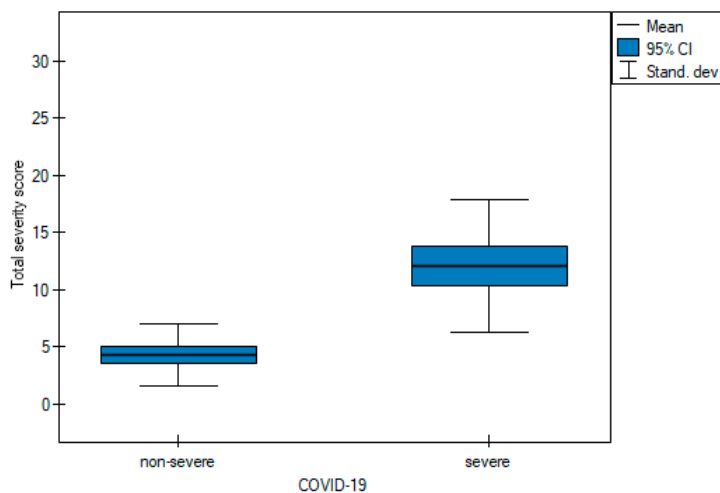


Figure 16. Box plot of comparisons of mean TSS for non-severe and severe COVID-19 patients.

A time consumption analysis (Table 6) of each of the three methods was used to decide which method should be chosen first.

Table 6. Comparisons of examination time in seconds of each of the three quantitative scoring systems.

Statistic	Interpretation Time [seconds]			p Value
	Chest CT Severity Score	Chest CT Score	Total Severity Score	
Average	35.32	35.62	29.86	0.002
Median	30	35	30	0.002
Q1-Q3	22.75-40	28-45	22-38	
Range	10-78	10-68	10-55	
Pairwise comparisons	B	B	A	

p value: Friedman test, Q1-Q3: the first quartile - the third quartile. Pairwise comparisons (Test POST-HOC Conover-Iman): similar letters = insignificant difference, different letters = significant difference.

3.4. Time Consumption

Table 6 shows the results obtained during the analysis, which was based on the average and median time of the study.

The results arranged from the longest to the shortest according to the average were as follows: Chest CT score_time > Chest CT severity score_time > Total severity score_time. The results arranged according to the median value: Chest CT score > Chest CT severity score = Total severity score. In addition, pairwise comparisons showed a statistically significant difference between all pairs except Chest CT severity score_time and Chest CT severity score_time, which ended up in the same group (B). Figure 17 shows box plots comparing the mean interpretation time of the three quantitative scoring systems, whereas Figure 18 compares the median time.

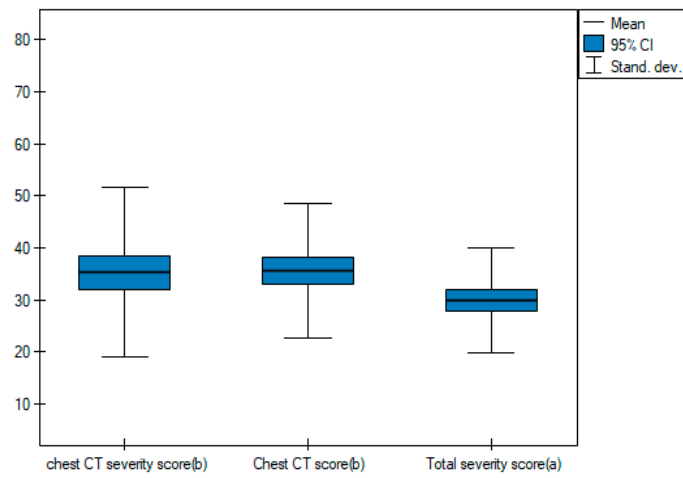


Figure 17. Box plot of comparisons of the mean interpretation times of the three quantitative scoring systems.

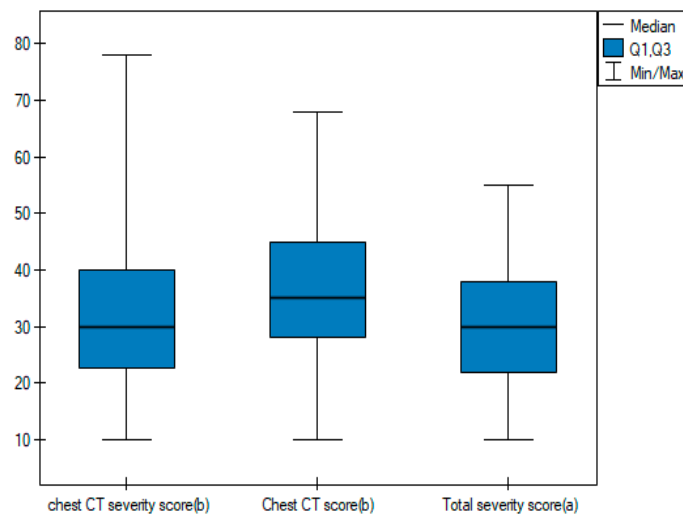


Figure 18. Box plot of comparisons of the median interpretation times of the three quantitative scoring systems.

Figures 19–21 illustrate typical manifestations of COVID-19 pneumonia in analyzed patients.

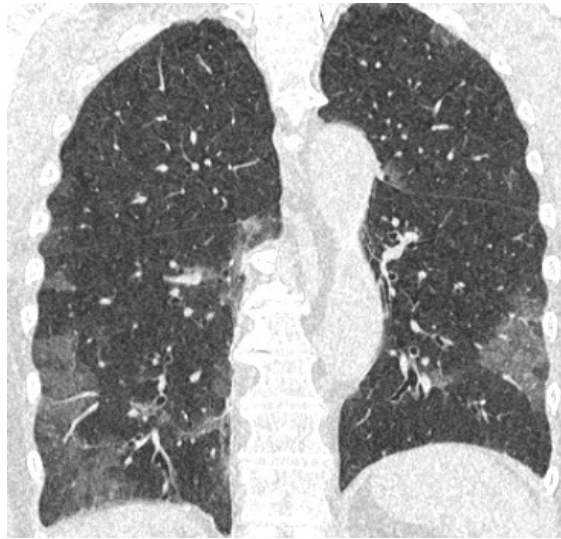


Figure 19. Coronal reconstruction of non-enhanced CT reveals bilateral ground glass opacities in peripheral distribution in lower lobes.



Figure 20. Axial plane of non-enhanced CT reveals bilateral ground glass opacities with superimposition of interlobular septal thickening, giving the crazy paving appearance, distributed symmetrically in both lungs.



Figure 21. Axial plane of non-enhanced CT reveals ground glass opacities in subpleural distribution in lower lobes.

4. Discussion

The role of chest CT in the pandemic era of COVID-19 has been established as an auxiliary method for assessing the severity and extent of lung involvement in a selected group of patients. The additional use of a scoring system for evaluation allows for more objective and standardized results and may also be useful as a short-term prognostic factor [14]. There have been several studies evaluating scoring systems in COVID-19 pneumonia in different groups of patients [5,6,11,14].

According to Tharwat et. al, TSS may have prognostic value in patients with acute renal failure or chronic kidney disease. Higher TSS scores and a predominant pattern of pulmonary consolidations were more common in patients in severe clinical condition ($p < 0.05$) [15]. These findings are consistent with our study, with significantly higher values in TSS in the severe COVID-19 group.

The m-TSS method was a qualitative method to distinguish the main radiological patterns present in COVID-19 pneumonia. Category A for the GGO pattern was the most common observation in our study and predominated in 58% of patients (Figures 19–21). GGO is not a feature specific to COVID-19 pneumonia and can occur in several conditions. In hematologic patients, the differential diagnosis of GGO should include other viral infections such as cytomegalovirus, alveolar hemorrhage, drug toxicity and organizing pneumonia [16]. Our study supports the results of the meta-analysis by Zheng et al., where GGO, vascular enlargement, alveolar septal thickening, and subpleural lines were the most common findings in both normal and severe patients [17]. Furthermore, our results presented excellent inter-observer agreement in qualitative analysis in the mTSS method ($p < 0.001$).

In a study by Yang et al., the threshold for identifying patients with severe infection in CT-SS was 19.5 with 83.3% sensitivity and 94% specificity [6]. In our study, the results for CT-SS were 14, 72.7%, and 98.2% respectively, confirming excellent diagnostic performance of the method. Additionally, the AUC values of analyzed semi-quantitative methods ranged between 0.881 and 0.902, suggesting that all of them can be considered as excellent tools for discriminating patients with severe and non-severe COVID-19 disease. In all semi quantitative methods, patients in the severe COVID-19 group received higher

scores than non-severe patients ($p < 0.005$). In the study by Li et al., patients with severe clinical conditions had significantly higher scores in the CT-S. Moreover, sensitivity, specificity, and cut-off values for identifying severe cases were 80%, 82.8%, and 7, respectively, whereas the AUC value for the ROC curve was 0.87 [18]. In our study, the values were as follows: 75%, 100%, and 14. The AUC value in the ROC curve was 0.899. Our results are similar, confirming very good diagnostic performance of this scale, even though the analyzed group was smaller. Another important point of analysis is the repeatability and feasibility of the method. In our study, we achieved excellent inter-observer reliability in all three semi quantitative methods with the ICC values > 0.9 .

During the pandemic era, several CT scales were invented to assess lung involvement in COVID-19 infection. In a recent study published in May 2022, Dilek et al. proposed an Early Decision Severity Score. The system includes evaluation of patients based on visual CT scorings, intubation necessities, and mortality rates. The combination of radiological and clinical factors had the additional benefit of assessing patient's prognosis [19]. In our study, several clinical parameters were analyzed.

Respiratory failure is one of the leading causes of COVID-19 mortality [20]. Patients with low oxygen saturation have a higher risk of death, which supports results that link hypoxemia to mortality [21]. In the analyzed group of patients, oxygen saturation varied significantly with the average values in non-severe and severe patients reaching 94% and 82%, respectively (Table 1 and Figure 1).

One of the laboratory parameters associated with mortality in patients with COVID-19 is D-dimer. D-dimer levels are elevated in patients of all age groups with COVID-19. In patients with COVID-19, the existence of a concomitant disease such as diabetes, cancer, stroke, and physiological conditions such as pregnancy may contribute to elevated D-dimer levels. On the other hand, the correlation between high D-dimer levels and survival rates underscores the importance of detecting D-dimer levels in patients with COVID-19 [22]. In our study, not surprisingly, D-dimer values were significantly higher in the severe COVID-19 group with the mean value of 3562 ug/L (Table 1 and Figure 2).

CRP levels were found to be significantly elevated in the initial phases of the infection in patients with severe COVID-19 also prior to indications of critical findings with CT. Importantly, CRP has been associated with disease progression and is an early predictor for severe COVID-19 [23]. In our study, patients in the severe COVID-19 group had significantly higher CRP levels in contrast to the non-severe COVID-19 group (Table 1 and Figure 3).

Compared to the general patient population, those with comorbidities have a poor prognosis and high mortality resulting from COVID-19 [24,25]. In hematological patients, advanced disease, older age, type of malignancy, and several laboratory parameters, such as high CRP, lymphopenia, and neutropenia have been correlated with COVID-19 mortality [26–28]. Chronic diseases such as diabetes or arterial hypertension are associated with a high mortality rate [29]. Our study supports those findings, with significantly higher mortality in patients with comorbidities, particularly in those with diabetes.

To the best of our knowledge, this is the first study analyzing diagnostic accuracy of chest CT scales in COVID-19 in hematology patients. A recent study by Elmokadem et al. analyzed the diagnostic performance of five different CT chest severity scoring systems in ordinary patients and found that Chest CT-SS had the highest specificity and utilized the least amount of time when compared to other scoring systems [30]. The results were concordant with our study, with 98.2% specificity for Chest CT-SS and excellent AUC values of 0.902 ($p < 0.001$). Interestingly, the median interpretation time in Chest CT-SS and TSS was equal, while in Chest CT-S, it was slightly longer ($p = 0.002$).

Our study has a few limitations. Firstly, as it was a single-center study, the group was relatively small and thus further studies with more patients are warranted. To confirm our results, larger datasets are needed. Secondly, patients suffered from different hematological malignancies at different stages of diseases. Taking this fact into account, some laboratory parameters could not be reliably interpreted and collected for analysis

due to different clinical stages of hematological disease. Furthermore, due to the retrospective nature of the study, some clinical data were incomplete and thus clinical analysis was very limited to selected laboratory parameters; however, we managed to collect one significant to assess prognosis and risk factors such as D-dimer and CRP.

5. Conclusions

The analyzed chest CT scores presented excellent inter-observer agreement. Chest CT score and chest CT severity score presented very high sensitivity and specificity in terms of diagnostic accuracy. The highest AUC values and shortest median times of analysis in chest CT severity scores suggests this method as the most comprehensive for semi-quantitative assessment of chest CT in hematological patients with COVID-19.

Author Contributions: Conceptualization, M.H.-R. and L.G.-D.; methodology, M.H.-R. and L.G.-D.; software, M.H.-R. and L.G.-D.; validation, M.H.-R., L.G.-D., J.D.-S. and M.J.; formal analysis, M.H.-R., L.G.-D. and J.D.-S.; investigation, M.H.-R., L.G.-D. and J.D.-S.; resources M.H.-R. and L.G.-D.; data curation, M.H.-R. and L.G.-D.; writing—original draft preparation, M.H.-R. and L.G.-D.; writing—review and editing, M.H.-R., L.G.-D. and M.J.; visualization, M.H.-R. and L.G.-D.; supervision, L.G.-D. and M.J.; project administration, M.H.-R. and L.G.-D. All authors have read and agreed to the published version of the manuscript.

Funding: This research received no external funding.

Institutional Review Board Statement: The study was conducted in accordance with the Declaration of Helsinki and approved by the Institutional Review Board of Medical University of Warsaw AKBE/297/2022 date 12.12.2022.

Informed Consent Statement: Not applicable.

Data Availability Statement: The data presented in this study are available in this article.

Conflicts of Interest: The authors declare no conflict of interest.

References

1. Leung, C. Risk factors for predicting mortality in elderly patients with COVID-19: A review of clinical data in China. *Mech. Ageing Dev.* **2020**, *188*, 111255.
2. Tagliamento, M.; Agostinetto, E.; Bruzzzone, M.; Ceppi, M.; Saini, K.S.; de Azambuja, E.; Punie, K.; Westphalen, C.B.; Morgan, G.; Pronzato, P.; et al. Mortality in adult patients with solid or hematological malignancies and SARS-CoV-2 infection with a specific focus on lung and breast cancers: A systematic review and meta-analysis. *Crit. Rev. Oncol. Hematol.* **2021**, *163*, 103365.
3. Mossa-Basha, M.; Meltzer, C.C.; Kim, D.C.; Tuite, M.J.; Kolli, K.P.; Tan, B.S. Radiology Department preparedness for COVID-19: Radiology Scientific Expert Panel. *Radiology* **2020**, *296*, E106–E112.
4. Cieszanowski, A.; Czekajka, E.; Giżycka, B.; Gruszczynska, K.; Oronowicz-Jaškowiak, A.S.; Podgórska, J.; Serafin, Z.; Szurowska, E.; Walecki, J. Indications for imaging studies in SARS-CoV-2 infected patients—Recommendations of the Polish Medical Society of Radiology. *Pol. J. Radiol.* **2022**, *87*, e63–e68.
5. Ai, T.; Yang, Z.; Hou, H.; Zhan, C.; Chen, C.; Lv, W.; Tao, Q.; Sun, Z.; Xia, L. Correlation of chest CT and RT-PCR testing in coronavirus disease 2019 (COVID-19) in China: A report of 1014 cases. *Radiology* **2020**, *296*, 200642.
6. Yang, R.; Li, X.; Liu, H.; Zhen, Y.; Zhang, X.; Xiong, Q.; Luo, Y.; Gao, C.; Zeng, W. Chest CT Severity Score: An Imaging Tool for Assessing Severe COVID-19. *Radiol. Cardiothorac. Imaging* **2020**, *2*, e200047.
7. Eshet, Y.; Avigdor, A.; Kedmi, M.; Tau, N. Imaging of Hematological Patients in the Era of COVID-19. *Acta Haematol.* **2022**, *145*, 267–274.
8. Flisiak, R.; Horban, A.; Jaroszewicz, J.; Kozielowicz, D.; Mastalerz-Migas, A.; Owczuk, R.; Parczewski, M.; Pawłowska, M.; Piekarska, A.; Simon, K.; et al. Management of SARS-CoV-2 infection: Recommendations of the Polish Association of Epidemiologists and Infectiologists as of April 26, 2021. *Pol. Arch. Intern. Med.* **2021**, *131*, 487–496.
9. Austin, J.H.; Muller, N.L.; Friedman, P.J.; Hansell, D.M.; Naidich, D.P.; Remy-Jardin, M.; Webb, W.R.; Zerhouni, E.A. Glossary of terms for CT of the lungs: Recommendations of the Nomenclature Committee of the Fleischner Society. *Radiology* **1996**, *200*, 327–331.
10. Pan, F.; Ye, T.; Sun, P.; Gui, S.; Liang, B.; Li, L.; Zheng, D.; Wang, J.; Hesketh, R.L.; Yang, L.; et al. Time course of lung changes on chest CT during recovery from 2019 novel coronavirus (COVID-19) pneumonia. *Radiology* **2020**, *295*, 715–721.
11. Francone, M.; Iafrate, F.; Masci, G.M.; Coco, S.; Cilia, F.; Manganaro, L.; Panebianco, V.; Andreoli, C.; Colaiacono, M.C.; Zingarepoli, M.A.; et al. Chest CT score in COVID-19 patients: Correlation with disease severity and short-term prognosis. *Eur. Radiol.* **2020**, *30*, 6808–6817.

12. Li, K.; Fang, Y.; Li, W.; Pan, C.; Qin, P.; Zhong, Y.; Liu, X.; Huang, M.; Liao, Y.; Li, S. CT image visual quantitative evaluation and clinical classification of coronavirus disease (COVID-19). *Eur. Radiol.* **2020**, *30*, 4407–4416.
13. Wasilewski, P.G.; Mruk, B.; Mazur, S.; Póltorak-Szymczak, G.; Sklinda, K.; Walecki, J. COVID-19 severity scoring systems in radiological imaging—A review. *Pol. J. Radiol.* **2020**, *85*, e361.
14. Aziz-Ahari, A.; Keyhanian, M.; Mamishi, S.; Mahmoudi, S.; Bastani, E.E.; Asadi, F.; Khaleghi, M. Chest CT severity score: Assessment of COVID-19 severity and short-term prognosis in hospitalized Iranian patients. *Wien. Med. Wochenschr.* **2022**, *172*, 77–83.
15. Tharwat, S.; Saleh, G.A.; Saleh, M.; Mounir, A.M.; Abdelzaher, D.G.; Salah, A.M.; Nassar, M.K. Chest CT Total Severity Score on Admission to Predict In-Hospital Mortality in COVID-19 Patients with Acute and Chronic Renal Impairment. *Diagnostics* **2022**, *12*, 1529.
16. Cozzi, D.; Cavigli, E.; Moroni, C.; Smorchkova, O.; Zantonelli, G.; Pradella, S.; Miele, V. Ground-glass opacity (GGO): A review of the differential diagnosis in the era of COVID-19. *Jpn. J. Radiol.* **2021**, *39*, 721–732.
17. Zheng, Y.; Wang, L.; Ben, S. Meta-analysis of chest CT features of patients with COVID-19 pneumonia. *J. Med. Virol.* **2021**, *93*, 241–249.
18. Li, K.; Wu, J.; Wu, F.; Guo, D.; Chen, L.; Fang, Z.; Li, C. The Clinical and Chest CT Features Associated with Severe and Critical COVID-19 Pneumonia. *Investig. Radiol.* **2020**, *55*, 327–331.
19. Dilek, O.; Demirel, E.; Akkaya, H.; Belibagli, M.C.; Soker, G.; Gulek, B. Different chest CT scoring systems in patients with COVID-19: Could baseline CT be a helpful tool in predicting survival in patients with matched ages and co-morbid conditions? *Acta Radiol.* **2022**, *63*, 615–622.
20. Lai, A.G.; Pasea, L.; Banerjee, A.; Hall, G.; Denaxas, S.; Chang, W.H.; Katsoulis, M.; Williams, B.; Pillay, D.; Noursadeghi, M.; et al. Estimated Impact of the COVID-19 Pandemic on Cancer Services and Excess 1-Year Mortality in People with Cancer and Multimorbidity: Near Real-Time Data on Cancer Care, Cancer Deaths and a Population-Based Cohort Study. *BMJ Open* **2020**, *10*, e043828.
21. Ferrer, R. COVID-19 Pandemic: The Greatest Challenge in the History of Critical Care. *Med. Intensiva.* **2020**, *44*, 323–324.
22. Rostami, M.; Mansouritorghabeh, H. D-dimer level in COVID-19 infection: A systematic review. *Expert Rev. Hematol.* **2020**, *11*, 1265–1275.
23. Tan, C.; Huang, Y.; Shi, F.; Tan, K.; Ma, Q.; Chen, Y.; Jiang, X.; Li, X. C-reactive protein correlates with CT findings and predicts severe COVID-19 early. *J. Med. Virol.* **2020**, *92*, 856–862.
24. Wang, C.; Horby, P.W.; Hayden, F.G.; Gao, G.F. A novel coronavirus outbreak of global health concern. *Lancet* **2020**, *395*, 470–473.
25. Bernheim, A.; Mei, X.; Huang, M.; Yang, Y.; Fayad, Z.A.; Zhang, N.; Diao, K.; Lin, B.; Zhu, X.; Li, K.; et al. Chest CT findings in coronavirus disease-19 (COVID-19): Relationship to duration of infection. *Radiology* **2020**, *295*, 200463.
26. García-Suárez, J.; de la Cruz, J.; Cedillo, A.; Llamas, P.; Duarte, R.; Jiménez-Yuste, V.; Hernández-Rivas, J.Á.; Gil-Manso, R.; Kwon, M.; Sánchez-Godoy, P.; et al. Impact of hematologic malignancy and type of cancer therapy on COVID-19 severity and mortality: Lessons from a large population-based registry study. *J. Hematol. Oncol.* **2020**, *13*, 133.
27. Piñana, J.L.; Martino, R.; García-García, I.; Parody, R.; Morales, M.D.; Benzo, G.; Gómez-Catalan, I.; Coll, R.; De La Fuente, I.; Luna, A.; et al. Risk factors and outcome of COVID-19 in patients with hematological malignancies. *Exp. Hematol. Oncol.* **2020**, *9*, 21.
28. Passamonti, F.; Cattaneo, C.; Arcaini, L.; Bruna, R.; Cavo, M.; Merli, F.; Angelucci, E.; Krampera, M.; Cairoli, R.; Della Porta, M.G.; et al. Clinical characteristics and risk factors associated with COVID-19 severity in patients with hematological malignancies in Italy: A retrospective, multicentre, cohort study. *Lancet Haematol.* **2020**, *7*, e737–e745.
29. Di Lorenzo, G.; Buonerba, L.; Ingenito, C.; Crocetto, F.; Buonerba, C.; Libroia, A.; Sciarra, A.; Ragone, G.; Sanseverino, R.; Iaccarino, S.; et al. Clinical Characteristics of Metastatic Prostate Cancer Patients Infected with COVID-19 in South Italy. *Oncology* **2020**, *98*, 743–747.
30. Elmokadem, A.H.; Mounir, A.M.; Ramadan, Z.A.; Elsedeiq, M.; Saleh, G.A. Comparison of Chest CT Severity Scoring Systems for COVID-19. *Eur. Radiol.* **2022**, *32*, 3501–3512.

Disclaimer/Publisher’s Note: The statements, opinions and data contained in all publications are solely those of the individual author(s) and contributor(s) and not of MDPI and/or the editor(s). MDPI and/or the editor(s) disclaim responsibility for any injury to people or property resulting from any ideas, methods, instructions or products referred to in the content.

7. Wnioski

1. Zastosowanie najnowszych kryteriów EORTC/MSG, rozszerzonych o nowe objawy radiologiczne istotnie wpłynęło na postępowanie kliniczne w badanej grupie pacjentów i zwiększyło wartość diagnostyczną wyjściowej tomografii komputerowej wysokiej rozdzielczości o 11,4% w rozpoznawaniu prawdopodobnej inwazyjnej aspergilozy płucnej.
2. Na podstawie analizy porównawczej skal stosowanych do oceny zaawansowania zmian zapalnych w miąższu płucnym w przebiegu COVID-19, można wnioskować, iż skala Chest CT Severity Score stanowi metodę rekomendowaną w grupie pacjentów z nowotworami hematologicznymi i COVID-19.

8. Opinie Komisji Bioetycznej



Komisja Bioetyczna przy Warszawskim Uniwersytecie Medycznym

Tel.: 022/ 57 - 20 -303

Fax: 022/ 57 - 20 -165

ul. Żwirki i Wigury nr 61

02-091 Warszawa

e-mail: komisja.bioetyczna@wum.edu.pl

www.komisja-bioetyczna.wum.edu.pl

Warszawa, dnia 12.12.2022r.

AKBE/ 294 / 2022

Lek. Marta Hałaburda-Rola
II Zakład Radiologii Klinicznej,
ul. Banacha 1a, 02-097 Warszawa

OŚWIADCZENIE

Niniejszym oświadczam, że Komisja Bioetyczna przy Warszawskim Uniwersytecie Medycznym w dniu 12 grudnia 2022r. przyjęła do wiadomości informację na temat badania pt. "Analiza porównawcza skan tomografii komputerowej nasilenia COVID-19 u pacjentów z chorobami hematologicznymi."

Przedstawione badanie nie stanowi eksperymentu medycznego w rozumieniu art. 21ust.1 ustawy z dnia 5 grudnia 1996 r. o zawodach lekarza i lekarza dentystry (Dz.U. z 2018 r.poz. 617) i nie wymaga uzyskania opinii Komisji Bioetycznej przy Warszawskim Uniwersytecie Medycznym, o której mowa w art. 29 ust.1 ww. ustawy.

Przewodnicząca Komisji Bioetycznej

Prof. dr hab. n. med. Magdalena Kuźma –Kozakiewicz



Komisja Bioetyczna przy Warszawskim Uniwersytecie Medycznym

Tel.: 022/ 57 - 20 -303
Fax: 022/ 57 - 20 -165

ul. Żwirki i Wigury nr 61
02-091 Warszawa

e-mail: komisja.bioetyczna@wum.edu.pl
www.komisja-bioetyczna.wum.edu.pl

Warszawa, dnia 17 stycznia 2022r.

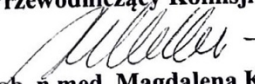
AKBE/44/2022

Lek. Marta Hałaburda-Rola
II Zakład Radiologii Klinicznej,
ul. Banacha 1a, 02-097 Warszawa

OŚWIADCZENIE

Niniejszym oświadczam, że Komisja Bioetyczna przy Warszawskim Uniwersytecie Medycznym w dniu 17 stycznia 2022r. przyjęła do wiadomości informację na temat badania pt:” Kliniczna użyteczność Tomografii Komputerowej wysokiej rozdzielczości –HR u pacjentów hematologicznych z Covid-19 do diagnozowania inwazyjnej aspergilozy płucnej.” (Clinical utility of high-resolution computed tomography in COVID-19 hematologic patients to diagnose invasive pulmonary aspergillosis.) Przedstawione badanie nie stanowi eksperymentu medycznego w rozumieniu art. 21 ust. 1 ustawy z dnia 5 grudnia 1996 r. o zawodach lekarza i lekarza dentystry(Dz.U. z 2018 r. poz. 617) i nie wymaga uzyskania opinii Komisji Bioetycznej przy Warszawskim Uniwersytecie Medycznym, o której mowa w art. 2 ust.1 ww. ustawy.

Przewodniczący Komisji Bioetycznej


Prof. dr hab. n.med. Magdalena Kuźma-Kozakiewicz

*niepotrzebne skreślić

9. Oświadczenia wszystkich współautorów publikacji określające indywidualny wkład każdego z nich w ich powstanie

Oświadczenia wszystkich współautorów cyklu publikacji stanowiących rozprawę doktorską, określające ich indywidualny wkład

Oświadczenia współautora publikacji stanowiących rozprawę doktorską

Dr hab. n. med. **Tomasz Dzieciatkowski** (Katedra i Zakład Mikrobiologii Lekarskiej, Warszawski Uniwersytet Medyczny) – nadzór merytoryczny nad prowadzeniem badania, wsparcie w opracowaniu metodologii, nadzór nad interpretacją otrzymanych wyników.

***Hałaburda-Rola M.** Dzieciatkowski T, Górka M, Rowiński O, Grabowska-Derlatka L. Clinical utility of the updated European Organization for Research and Treatment of Cancer/Invasive Fungal Infections Cooperative Group and the National Institute of Allergy and the Mycoses Study Group Education and Research Consortium computed tomography criteria of invasive pulmonary aspergillosis in hematological malignancies. *Hematology*. 2021 Dec;26(1):398-407. doi: 10.1080/16078454.2021.1931739.*

Mój udział procentowy w przygotowaniu publikacji określam jako 8%

Wyrażam zgodę na wykorzystanie w/w pracy jako część rozprawy doktorskiej lek. Marty Hałaburdy-Rola.

Katedra i Zakład Mikrobiologii Lekarskiej



dr hab. n. med. Tomasz Dzieciatkowski

Oświadczenia wszystkich współautorów cyklu publikacji stanowiących rozprawę doktorską, określające ich indywidualny wkład

Oświadczenia współautora publikacji stanowiących rozprawę doktorską

Lek. **Michał Górka** (Katedra i Klinika Hematologii, Transplantologii i Chorób Wewnętrznych, Warszawski Uniwersytet Medyczny) – wsparcie merytoryczne nad prowadzeniem badania.

***Hałaburda-Rola M**, Dzieciatkowski T, Górka M, Rowiński O, Grabowska-Derlatka L. Clinical utility of the updated European Organization for Research and Treatment of Cancer/Invasive Fungal Infections Cooperative Group and the National Institute of Allergy and the Mycoses Study Group Education and Research Consortium computed tomography criteria of invasive pulmonary aspergillosis in hematological malignancies. Hematology. 2021 Dec;26(1):398-407. doi: 10.1080/16078454.2021.1931739.*

Mój udział procentowy w przygotowaniu publikacji określam jako 1%

Wyrażam zgodę na wykorzystanie w/w pracy jako część rozprawy doktorskiej lek Marty Hałaburdy- Rola.

Lekarz Michał Górka
specjalista chorób wewnętrznych
specjalista hematologii
2649806

Oświadczenia współautora publikacji stanowiących rozprawę doktorską

Dr n. med. **Joanna Drozd- Sokołowska** (Katedra i Klinika Hematologii, Transplantologii i Chorób Wewnętrznych, Warszawski Uniwersytet Medyczny) – udostępnienie miejsca i sprzętu do przeprowadzenia badania, nadzór nad przygotowaniem manuskryptu.

Hałaburda-Rola M, Drozd-Sokołowska J, Januszewicz M, Grabowska-Derlatka L. *Comparison of Computed Tomography Scoring Systems in Patients with COVID-19 and Hematological Malignancies. Cancers.* 2023; 15(9):2417. <https://doi.org/10.3390/cancers15092417>

Mój udział procentowy w przygotowaniu publikacji określam jako 8%

Wyrażam zgodę na wykorzystanie w/w pracy jako część rozprawy doktorskiej lek Marty Hałaburdy- Rola.

Joanna Drozd- Sokołowska

**Oświadczenia wszystkich współautorów cyklu publikacji stanowiących
rozprawę doktorską, określające ich indywidualny wkład**

Oświadczenia współautora publikacji stanowiących rozprawę doktorską

Prof. dr hab. n. med. **Olgierd Rowiński** (II Zakład Radiologii Klinicznej, Warszawski Uniwersytet Medyczny) –udostępnienie miejsca i sprzętu do przeprowadzenia badania, nadzór nad przygotowaniem manuskryptu.

***Hałaburda-Rola M**, Dzieciatkowski T, Górka M, Rowiński O, Grabowska-Derlatka L. Clinical utility of the updated European Organization for Research and Treatment of Cancer/Invasive Fungal Infections Cooperative Group and the National Institute of Allergy and the Mycoses Study Group Education and Research Consortium computed tomography criteria of invasive pulmonary aspergillosis in hematological malignancies. Hematology. 2021 Dec;26(1):398-407. doi: 10.1080/16078454.2021.1931739.*

Mój udział procentowy w przygotowaniu publikacji określám jako 1%

Wyrażám zgodę na wykorzystanie w/w wymienionej pracy jako część rozprawy doktorskiej
lek Marty Hałaburdy- Rola.

Uniwersyteckie Centrum Kliniczne
Warszawskiego Uniwersytetu Medycznego
Centralny Szpital Kliniczny
II Zakład Radiologii Klinicznej
02-097 Warszawa, ul. S. Banacha 1a
NIP 522-00-02-529, REGON 000288975-00030
tel. 22 599 23 00, fax: 22 599 23 02

KIEROWNIK
II Zakładu Radiologii Klinicznej
Prof. nadzw. dr hab. n. med.
Olgierd Rowiński

**Oświadczenia wszystkich współautorów cyklu publikacji stanowiących
rozprawę doktorską, określające ich indywidualny wkład**

Oświadczenia współautora publikacji stanowiących rozprawę doktorską

Dr hab. n. med. **Magdalena Januszewicz** (II Zakład Radiologii Klinicznej,
Warszawski Uniwersytet Medyczny) –udostępnienie miejsca i sprzętu do
przeprowadzenia badania, nadzór nad przygotowaniem manuskryptu.

Hałaburda-Rola M, Drozd-Sokołowska J, Januszewicz M, Grabowska-Derlatka L.
*Comparison of Computed Tomography Scoring Systems in Patients with COVID-19 and
Hematological Malignancies. Cancers.* 2023; 15(9):2417.
<https://doi.org/10.3390/cancers15092417>

Mój udział procentowy w przygotowaniu publikacji określam jako 1%

Wyrażam zgodę na wykorzystanie w/w pracy jako część rozprawy doktorskiej lek Marty
Hałaburdy- Rola.

Uniwersyteckie Centrum Kliniczne
Warszawskiego Uniwersytetu Medycznego
Centralny Szpital Kliniczny
II Zakład Radiologii Klinicznej
02-097 Warszawa, ul. S. Banacha 1a
NIP 522-00-02-529, REGON 000288975-00030
tel. 22 599 23 00, fax: 22 599 23 02

KIEROWNIK
II Zakładu Radiologii Klinicznej
Centralny Szpital Kliniczny UCK WUM
dr hab. n. med. Magdalena Januszewicz



Oświadczenia wszystkich współautorów cyklu publikacji stanowiących rozprawę doktorską, określające ich indywidualny wkład

Oświadczenia współautora publikacji stanowiących rozprawę doktorską

Dr hab. n. med. **Laretta Grabowska- Derlatka** (II Zakład Radiologii Klinicznej, Warszawski Uniwersytet Medyczny) – nadzór merytoryczny nad prowadzeniem badania, opracowanie metodologii, nadzór nad interpretacją otrzymanych wyników, pisanie artykułów stanowiących cykl publikacji.

Hałaburda-Rola M, Dzieciatkowski T, Górka M, Rowiński O, Grabowska-Derlatka L. *Clinical utility of the updated European Organization for Research and Treatment of Cancer/Invasive Fungal Infections Cooperative Group and the National Institute of Allergy and the Mycoses Study Group Education and Research Consortium computed tomography criteria of invasive pulmonary aspergillosis in hematological malignancies. Hematology. 2021 Dec;26(1):398-407. doi: 10.1080/16078454.2021.1931739.*

Mój udział procentowy w przygotowaniu publikacji określam jako 20%

Hałaburda-Rola M, Drozd-Sokołowska J, Januszewicz M, Grabowska-Derlatka L. *Comparison of Computed Tomography Scoring Systems in Patients with COVID-19 and Hematological Malignancies. Cancers. 2023; 15(9):2417. <https://doi.org/10.3390/cancers15092417>*

Mój udział procentowy w przygotowaniu publikacji określam jako 20%

Wyrażam zgodę na wykorzystanie w/w prac jako część rozprawy doktorskiej lek Marty Hałaburdy- Rola.

dr hab. n. med.
LARETTA GRABOWSKA-DERLATKA
specjalista radiolog
2190959